This is a preprint, the final version is subject to change, of the American Mineralogist (MSA)
Cite as Authors (Year) Title. American Mineralogist, in press.
DOI: https://doi.org/10.2138/am-2020-7114

Revision 1

Reaction between Cu-bearing minerals and hydrothermal fluids at 800°C and 200 MPa: constraints from synthetic fluid inclusions

Dongmei Qi[1*], Harald Behrens[1], Roman Botcharnikov[1,2], Insa Derrey[1],

Francois Holtz[1], Chao Zhang[1], Xiaoyan Li[1], Ingo Horn[1]

[1]Institut für Mineralogie, Leibniz Universität Hannover, Callinstraße 3, Hannover,

D-30167, Germany

[2]Institut für Geowissenschaften, Johannes Gutenberg Universität Mainz,

J.-J.-Becher-Weg 21, Mainz, D-55128, Germany

(*corresponding author: dongmei.qi@xju.edu.cn)

This is a preprint, the final version is subject to change, of the American Mineralogist (MSA)
Cite as Authors (Year) Title. American Mineralogist, in press.
DOI: https://doi.org/10.2138/am-2020-7114

Abstract

Transport and deposition of copper in the Earth's crust are mainly controlled by the solubility of Cu-bearing phases and the speciation of Cu in magmatic-hydrothermal fluids. To improve our understanding of copper mobilization by hydrothermal fluids, we conducted an experimental study on the interaction between Cu-bearing phases (metallic copper, Cu_2O, CuCl) and aqueous chloride solutions (H_2O ± NaCl ± HCl; with Cl concentration of 0 to 4.3 mol kg^{-1}). The experiments were run in rapid heat/rapid quench cold seal pressure vessels at 800°C, 200 MPa and logfO_2 ~ NNO + 2.3. Either Cu capsules or Au capsules were used as containers. The reaction products were sampled *in situ* by the entrapment of synthetic fluid inclusions in quartz. Fluid composition was subsequently determined by analyzing individual fluid inclusions using a freezing cell and laser ablation inductively coupled plasma mass spectrometry. Our results show that large isolated and isometric inclusions, free of late stage modifications, can be preserved after experiment even when using a high cooling rate of 25 K s^{-1}.

The obtained results demonstrate that: (i) reaction between native Cu, NaCl solution and quartz (+/- silica gel) leads to the coexistence of fluid inclusions and Na-bearing silicate melt inclusions. Micrometer- to submicrometer-sized cuprite (Cu_2O) crystals have been observed in both types of the inclusions and they are formed most probably due to the dissociation of CuOH. (ii) When Cu^0 reacts with HCl and CuCl solutions, or Cu^+ reacts with NaCl solution, nantokite (CuCl) has been found in the fluid inclusions which was

formed due to oversaturation. Copper concentration in the fluid shows a strong positive dependence on the initial chlorine content, with Cu/Cl molal ratio varying from 1:9 to 1:1 in case (i) and (ii), respectively. When Cl is fixed to 1.5 m, initial fluid acidity has a major control on the Cu content, i.e., 0.17±0.09 m and 1.29±0.57 m Cu were measured in fluids of case (i) and (ii), respectively. Cu solubility in pure water and in 1.5 m NaCl solutions are 0.004±0.002 m and 0.16±0.07 m, respectively. The main responsible Cu-bearing complexes are $CuOH(H_2O)_x$ in water, $NaCuCl_2$ in NaCl solutions and $HCuCl_2$ in alkali-free solutions. These results provide quantitative constraints on the mobility of Cu in hydrothermal solutions and confirm that Cl is a very important ligand responsible for Cu transport. The first observation that silicate melt can be generated in the fluid-dominated and native-copper-bearing system implies that transitional thermosilicate liquids can coexist with metal-rich fluids and may enhance Cu mobility in magmatic-hydrothermal systems. This may have important implications for the formation of Cu deposits in the systems with low S activity.

Keywords

Synthetic fluid inclusions, silicate melt inclusions, native copper, cuprite, nantokite, quench rate, proper sealing

This is a preprint, the final version is subject to change, of the American Mineralogist (MSA)
Cite as Authors (Year) Title. American Mineralogist, in press.
DOI: https://doi.org/10.2138/am-2020-7114

1. Introduction

Formation of hydrothermal ore deposits requires a fluid with the ability to transport and deposit metals. Sources as well as physical and chemical characteristics of these hydrothermal fluids may vary widely (Bodnar et al., 2014). Fluid inclusions (FIs) trapped in minerals provide the most direct constraints on the composition of hydrothermal fluids responsible for mineralization and deposition of metals. However, an interpretation of natural observations requires calibration in the laboratory using synthetic fluid inclusions produced at controlled experimental conditions (Nash, 1976).

The valence state of copper is widely accepted as monovalent Cu^+ in silicate melts (e.g., Candela and Holland, 1984; Ripley and Brophy, 1995; Holzheid and Lodders, 2001; Zajacz et al., 2012), as well as in magmatic hydrothermal fluids (e.g., Fulton et al., 2000; Brugger et al., 2007; Schmidt et al., 2018). Both experimental and thermodynamic data show that magmatic hydrothermal fluids containing ligands like Cl^- and HS^- are the most important transport agents for Cu (e.g. Seward and Barnes, 1997; Liu and McPhail, 2005). Cuprous bisulfide complexes are stable under reduced conditions in near neutral to alkaline fluids with high total S concentrations (Crerar and Barnes, 1976; Thompson and Helz, 1994; Mountain and Seward, 1999, 2003). At high temperatures (>300°C), chlorine is the dominant Cu ligand in fluids (Mountain and Seward, 2003). Experimental investigations of Cu speciation in fluids at temperatures below 500°C (Crerar and Barnes, 1976; Var'yash, 1992; Xiao et al., 1998; Fulton et al., 2000; Archibald et al., 2001; Brugger et al., 2001;

Liu et al., 2001，2002; Berry et al., 2006; Sherman, 2007; Rempel et al., 2012) indicate that $[CuCl]^0$ and $[CuCl_2]^-$ complexes dominate in a wide range of Cl concentrations. Higher order complexes with the stoichiometry of $CuCl_n^{1-n}$ (where n>2) and $Cu_3Cl_3 \cdot (H_2O)_n$ are also considered to be possible complexes in vapor as well as in highly saline fluids (Xiao et al., 1998; Archibald et al., 2002; Williams-Jones et al., 2002; Liu et al., 2002, 2008).

The available synthetic FI studies on Cu solubility in hydrothermal brines in the single fluid phase region are generally focused on cuprous (e.g., Cu_2O) and/or cupric (e.g., $CuCl_2$) phases (e.g., Berry et al., 2006; Hack and Mavrogenes, 2006). Based on the analysis of synthetic FIs, Hack and Mavrogenes (2006) studied the influence of Cl concentration, temperature, and pressure on copper solubility at buffered oxygen fugacity and pH. The authors analyzed FIs with laser ablation inductively coupled plasma mass spectrometry (LA-ICP-MS) and measured up to 15 wt% Cu at 630°C and 340 MPa. Hack and Mavrogenes (2006) inferred high order complexes with general stoichiometry $CuCl(HCl)_{n-1}^0$ (where n is up to 4), preferring $n \leq 2$ at geological conditions. Berry et al. (2006) used XANES spectroscopy to extend the synthetic FI study of Hack and Mavrogenes (2006) by including native copper as a starting material. Their LA-ICP-MS and PIXE analyses indicated that ~10 wt% Cu was dissolved in the fluid (700°C and 341 MPa; 4-8 m KCl) which was equilibrated with native copper and mineral buffers. Berry et al. (2006) concluded that Cu^+ occurs as a linear species $[CuCl_2]^-$ in the presence of K^+ and as $[CuCl_4]^{3-}$ in the absence of K^+. Zajacz et al. (2011) conducted experiments in $Au_{97}Cu_3$ alloy capsules

(a_{Cu}=0.01) with various chemical components at 1000°C and 150 MPa. A maximum Cu content of 0.025 wt% was reached in 0.75 m NaCl solution. Zajacz et al. (2011) proposed the presence of $NaCuCl_2$ and $KCuCl_2$ complexes. There is a general agreement that Cu(I) remains stable at high temperatures, however, the change in redox state of Cu during reaction between native Cu and cuprous Cu at magmatic-hydrothermal conditions is not well understood.

Occurrence of native copper has been observed in several localities, such as in ancient oceanic pillow basalts (Nagle et al., 1973), in continental flood basalts (e.g., Stoiber and Davidson, 1959; Pinto et al., 2011; Zhang et al., 2013; Ikehata et al., 2016), and in mantle derived peridotites (Zhang et al., 2006; Ikehata and Hirata, 2012). In hydrothermal systems native copper can be concentrated to economic levels, such as in the world's largest and most significant Keweenaw Peninsula native copper ore district in USA, to a lesser extent in the Emeishan large igneous province in China, (e.g. Butler and Burbank, 1929; Zhu et al., 2003; Wang et al., 2006; Bornhorst and Mathur, 2017). However, the reaction mechanism of native copper with hydrothermal fluids has not been systematically studied at elevated temperatures and pressures. Thus, we conducted a detailed study of the behavior of copper in water and chlorine-bearing fluids at magmatic-hydrothermal conditions. Experiments were performed at 800°C and 200 MPa to equilibrate Cu-bearing minerals (Cu, Cu_2O and CuCl) containing different Cu species with aqueous hydrothermal fluids containing 0 to 4 mol Cl^- per kg H_2O, adjusted by addition of NaCl-, HCl- and CuCl-

bearing solutions. The equilibrated fluids were trapped *in situ* as FIs in quartz seed crystals. FIs were analyzed by laser ablation ICP-MS using freezing cell and femtosecond laser.

2. Experimental and analytical procedure

2.1 Experimental strategy

Three sets of experiments were performed at 800°C and 200 MPa (Table 1). Set 1 (System: ± Cu ± Cu_2O + NaCl): NaCl was added to evaluate the role of ligands which are charge-compensated by alkali; copper source was either metallic copper or cuprite. Set 2 (System: Cu ± Cu_2O ± CuCl ± HCl): Ligands for complex formation were added either as HCl or as CuCl. When using Cu tubes both components are equivalent since CuCl is present at run conditions (more details are given below). Using these two starting components (Cu and HCl) the role of hydrogen permeation through the capsule wall can be evaluated. Set 3: Experiments were designed for methodological reasons. The solubility of Cu in H_2O is probed in the absence of chloride in runs DQ-37A, B, C. The difference among these runs are that DQ-37A was loaded with Qz, and quench fluid was not extracted. DQ-37B, C were not loaded with Qz and quench fluids were extracted after 19 and 26 h, respectively. DQ-99, 100, 101 were performed to test whether measured composition of fluids in inclusions is consistent with the starting composition of the aqueous solution. DQ-124 was a test to check whether fluid components can leak into/out of inclusions during D_2O-H_2O exchange process. A pre-run was required (DQ-121), and FIs were first synthesized using a 1.5 m NaCl solution in a Cu capsule for 6 d. The retrieved quartz

cylinders were then transferred into a new Au capsule which was only loaded with pure D_2O prior to the run (DQ-124). Subsequently, the capsule was heated at the same condition for an hour. After this run, synthetic FIs were analyzed with Raman spectrometry and Fourier transform infrared spectroscopy to characterize the abundance of H_2O and D_2O qualitatively.

2.2 Starting materials and fluid inclusion synthesis

Quartz cylinders with a diameter of 2.0 mm, ca. 3 mm in length, and a weight of ca. 0.025 g, were drilled out parallel to the c-axis of a large, inclusion-free synthetic single crystal. After drilling, these cylinders were cleaned with acetone and distilled water in an ultrasonic bath.

Two techniques of FI entrapment were used in this study: 1) entrapment in pre-fractured quartz (hereafter denoted as pref. Qz); and 2) entrapment in the originally intact quartz which was cracked *in situ* during the experiment (denoted as *in situ* fractured quartz or i.s. Qz). The cracks are needed to provide space for FIs within the quartz crystal. The pref. Qz was prepared by heating at 350°C for 10 min in an atmospheric oven and quenching in distilled water. After drying, these quartz cylinders were immersed in 40% hydrofluoric acid for 10 min to leach quartz along the cracks, which helps to produce large and more abundant FIs, as suggested by Derrey et al. (2017). After leaching, the pre-fractured quartz cylinders were cleaned in acetone and distilled water to remove acid and

other possible contamination. Both pref. Qz and intact quartz cylinders were placed in an oven at 110°C overnight to remove all residual water from the surface and cracks.

Copper tubing was purchased from Sürth Stahl-Metalle und Schrauben, with a purity of 99.97 wt% Cu. Copper(I) oxide powder (purity of 97%, purchased from Sigma Aldrich) was directly used as a starting material or it was transformed into pellets by sintering. In doing so, cuprite (Cu_2O) powder (~1g) was pressed into pellet of 13 mm in diameter and 2 mm in thickness using the uniaxial pressing method at 140 MPa. Afterwards, these pellets were sintered at 1030°C for 30 h at atmospheric conditions, i.e. in the stability field of cuprite (Neumann et al., 1984).

NaCl solutions were prepared using distilled water and NaCl powder (purity of 99.99%, purchased from Alfa Aesar). HCl solutions were diluted from a 6 mol l^{-1} HCl stock solution. All solutions were doped with 400 - 600 μg g^{-1} RbCl and CsCl for internal standardization of LA-ICP-MS measurements (Duc-Tin et al., 2007; Derrey et al., 2017). Silica gel (purity of 99.99%) and Cu(I)Cl powder (purity of 99.999%) were purchased from Alfa Aesar. It must be noted that silica gel is generally added to the starting material unless otherwise mentioned. Further details about each proportion of the starting materials are provided in supplementary Table A1.

A schematic drawing of the assemblage in the capsule is shown in Fig.1a, and experimental details are listed in Table 1. Two types of capsules were used in this study, Cu capsules (2.45 mm I.D., 2.55 mm O.D. and 30 mm length) and Au capsules (2.80 mm

157 I.D., 3.20 mm O.D. and 30 mm length). Solutions ($H_2O \pm NaCl \pm HCl$; doped with internal
158 standards) and solid reactants (fine silica gel / quartz powder / CuCl powder / Cu_2O powder
159 / sintered Cu_2O pellet) were placed at the bottom of the capsule which was welded shut on
160 one end prior to loading. The total volume of liquid in the capsule was calculated to be
161 lower than the free volume in the capsule under experimental P, T conditions using the
162 equation from Pitzer and Sterner (1994) for pure H_2O. The capsules were crimped at the
163 center, and then two quartz cylinders were loaded in the upper part of the capsule. The
164 intact quartz cylinder was always placed beneath the pre-fractured quartz cylinder (Fig. 1a).
165 Capsules were squeezed on top, weighed, cut and then welded shut under Ar flow. During
166 welding, the capsule was cooled with a wrapped tissue soaked with distilled water and then
167 frozen by liquid nitrogen to avoid loss of volatile components during welding. The capsule
168 was weighed again to check for volatile loss during welding, stored in an oven at 110°C
169 overnight, and weighed a third time to test for possible leakage.

170 A rapid heat/rapid quench argon cold seal pressure vessel (RH/RQ Ar-CSPV, similar
171 to those described by Matthews et al. (2003)) was used for the experiments. All
172 experiments were conducted at 800°C and 200 MPa. Based on calibration, the uncertainties
173 of temperature and pressure measurements are $\leq \pm 5$°C and $\leq \pm 5$ MPa, respectively. Inside
174 a capsule filled with pure water (water activity equals to1), the oxygen fugacity imposed
175 by the vessel was ca. NNO + 2.3 (2.3 log units above the Ni-NiO buffer; Berndt et al.
176 (2001)). Loaded capsules were firstly pressurized to 200 MPa at room temperature and

177 then rapidly moved to the preheated hot zone of the vessel by an externally mobile magnet.
178 The heating of the capsules to 800°C occurred within few minutes at isobaric conditions.

179 Almost all experiments included an "intermediate quench" step (after 2-4 days, Table
180 1) by descending the sample to the water-cooled region to initiate cracks within the intact
181 quartz cylinder as a result of thermal stress (e.g., Li and Audétat, 2009). After intermediate
182 quench (< 20 s) the capsules were rapidly placed back in their previous position in the hot
183 zone (see Fig. 1b). In general, the technique to trap fluid at run conditions in synthetic FIs
184 in quartz follows the procedure of Bodnar and Sterner (1987) and Derrey et al. (2017) but
185 in this study five types of quench techniques were tested to optimize number and quality
186 of trapped FIs (Fig.1b):

187 [1] *Slow quench* (SQ) was used to avoid cracking of the quartz cylinders after the
188 experiment due to thermal shock. The autoclave was pulled out of the hot furnace and
189 cooled slowly to ambient conditions. The initial cooling rate of SQ is about 0.5 K s^{-1} (heavy
190 dashed line in Fig.1b) as estimated by the temperature evolution from target temperature
191 down to 300°C measured with the calibration unit and the outer thermocouple. The SQ
192 quench was applied in most of the synthetic FI studies.

193 [2] *Slow quench + rapid quench* (SQ+RQ) were conducted to avoid any entrapment of FIs
194 at low temperature in the late stages of the experiment. This technique was conducted in
195 two steps: firstly, the autoclave was removed out of the hot furnace, and the samples
196 remained in the hot part of the autoclave (as in case [1]); secondly, when the autoclave

197 temperatures reached 600°C, the sample was rapidly cooled by pulling it into the water-
198 cooled part of the autoclave. The cooling rates for these two stages were estimated to be 2
199 K s^{-1} (800-600°C) and ~25 K s^{-1} (600-300°C; light gray dashed line in Fig.1b), respectively.
200 [3] *Very slow quench + rapid quench* (VSQ+RQ) were only performed in HCl-bearing
201 system to test whether the number of inclusions could be increased. The sample was cooled
202 slowly from 800°C to 600°C at constant pressure by adjusting the cooling rate of the
203 furnace to 0.07 K s^{-1} (thin gray line in Fig.1b). After cooling to 600°C the sample was
204 quenched rapidly (RQ, see below). In this case the rapid quench was within the stability
205 field of α-quartz (< 630°C at 200 MPa; Swamy et al. (1994)).
206 [4] *Compressed air quench* (CAQ) was applied to adjust an intermediate cooling rate of
207 about 3 K s^{-1} (gray line in Fig.1b). The autoclave was pulled out of the furnace and
208 immediately cooled down by compressed air at the hot end.
209 [5] *Rapid quench* (RQ) revealed the highest cooling rate (thick black line in Fig.1b),
210 initiated by dropping the external magnet rapidly to place the sample at water-cooled zone.
211 Cooling rate for this procedure was determined to be ~25 K/s using the geospeedometer of
212 Zhang et al. (2000) based on water speciation in rhyolitic melts. In doing so, a ~30 mg
213 fragment of synthetic rhyolitic glass containing ~ 5 wt% H_2O was loaded in an Au capsule,
214 pre-equilibrated for a few minutes at 800°C and 200 MPa and then quenched rapidly. Water
215 speciation was measured by near-infrared spectroscopy.

After the experiment, the capsules were cleaned and weighed to verify that they had no leaks. Most capsules were squeezed, and the acidity of the fluid was tested with pH paper. Only two capsules (DQ-165 and DQ-169) were inflated but the weight was the same as before experiment. Inflation may have been caused by contamination with organic material during loading and formation of CO_2 at high temperature or by entrapment of Ar through small microcracks in the capsule wall, which were sealed by alloying during heating. Quench fluid extraction from the inflated capsules includes the following steps: (i) capsules were wrapped with a tissue soaked with distilled water and were frozen by liquid nitrogen; (ii) a small hole was pierced at the top, the tissue was removed and the capsule was allowed warming to room temperature before the quench fluid was extracted by a metal syringe; (iii) after transfer of the quenched fluid (~30 mg) into a Teflon vial, the capsule was rinsed with 1 ml deionized water. Half of the aliquots (~0.5 ml) was transferred to a new tube for pH determination (using an Inlab microelectrode). The residuals were weighed again and evaporated to dryness on a 90°C hotplate. The evaporated dryness was processed by following the procedure of Roebbert et al. (2018) for ICP-OES analyses. (iv) The final pH and elements concentration are calculated based on the dilution factor.

Quartz cylinders were removed from the capsules, mounted in epoxy resin and polished from both sides to a thickness of ca. 300 μm. The polishing allowed for easy identification of FIs under the microscope, and for the microthermometry measurements and analyses by LA-ICP-MS.

This is a preprint, the final version is subject to change, of the American Mineralogist (MSA)
Cite as Authors (Year) Title. American Mineralogist, in press.
DOI: https://doi.org/10.2138/am-2020-7114

2.3 Microthermometry and chemical analyses

Microthermometry was carried out on a *Linkam THMSG 600* heating (T < 600°C) and freezing stage. The in-house synthesized standard FIs (pure water-bearing and CO_2-bearing inclusions) were used to calibrate the stage, and the stage is accurate to ± 0.1°C in the range of -56.6°C to 0.0°C, and ± 1°C up to 347°C. Typically five FIs were analyzed in each quartz chip. Final ice melting temperatures (T_m) were determined to obtain bulk salinity (i.e. $NaCl_{eq.}$) of the fluids. Homogenization temperatures (T_h) were acquired by heating up the inclusions until a uniform phase was observed. Heating and cooling were repeated to check for reproducibility. The computer program BULK (Bakker, 2003) was used to estimate the bulk salinity of the FI.

The inclusions were analyzed for their major and minor element contents by LA-ICP-MS. An in-house built laser ablation system based on a UV-femtosecond-laser (*Spectra Physics*) was combined with a heating-freezing cell and a fast scanning sector field inductively coupled plasma mass spectrometer (*Element XR, Thermo Scientific*) (for more details see Albrecht et al. (2014)). The laser system operated in the deep UV at 194 nm and spot size was set to ca. 25 μm. The ablation cell was a modified INSTEC^{TM} heating-freezing stage with an adjusted volume of 3 cm^3. Helium mixed with 2 vol% hydrogen (to adjust the hydrogen flow rate to ca. 5-6 ml min^{-1}, as suggested by Guillong and Heinrich (2007)), was used as sample-chamber gas. After leaving the sample chamber, the gas was mixed with argon used as a carrier gas. Analyses were performed at a temperature of -40°C,

guaranteeing completely frozen FIs prior to the ablation, which resulted in an excellent control on the opening of the inclusions and considerably longer signal analysis time compared to the analysis of liquid FIs. Representative examples of FI analyses are shown in Fig. 2.

The analytical uncertainty of the method is estimated to be 10-30% for most studied elements as discussed in Albrecht et al. (2014). NIST SRM 610 glass was used as external standard (using reference values of the GeoReM database; Jochum et al., 2005), measured with a repetition rate of 10 Hz. The usual size of ablated inclusions was <25 μm, and laser repetition rates have been adjusted between 5 and 10 Hz, with higher rates for deeper (down to 40 μm) and lower rates for shallower (down to 20 μm) FIs. In some cases (DQ36-1 and DQ43-2), inclusions larger than 25 μm were ablated with the help of a Linux controlled ablation system. Here, inclusions were ablated spirally at repetition rates higher than 100 Hz. Both spot and spiral laser ablation signals have been compared in Fig.2. It is evident that the signal intensity is not affected by inclusion size (Fig.2-a, 2-b), and small FIs (e.g., 9 μm) can yield high signal intensities and good quality data. It has to be mentioned that the selected spot size on the sample surface was always bigger than the analyzed FI in order to guarantee that the whole FI is ablated and subsequently transported to the ICP-MS.

To evaluate the acquired data, the SILLS data reduction software designed by Guillong et al. (2008) was applied. The known initial Rb content was used for internal standardization of Cu±CuCl±Cu_2O±HCl and Cu_2O+NaCl systems, and the

276 microthermometrically determined Na content was used for the Cu+NaCl system (Table 2;
277 more details are given below).

278 The element contents of quench fluids were analyzed by inductively coupled plasma
279 optical emission spectrometry (ICP-OES) on a Varian Vista Pro system (Varian GmbH,
280 Germany).

281 Raman spectroscopy was used to identify trapped minerals and fractions of H_2O and
282 D_2O in inclusions. The measurements were performed using a confocal Bruker Senterra
283 micro-Raman spectrometer equipped with an Olympus BX 51 microscope and an Andor
284 DU420-OE CCD camera. Unpolarized spectra were collected under ambient conditions,
285 using the 532 nm laser excitation line with 20 mW power, and a long distance Olympus
286 50× magnification objective. Spectra were recorded for 10 s with 2 times acquisition
287 repetitions. Instrumental precision was within ±3 cm^{-1}.

288 IR spectra were collected with a Bruker IFS88 FTIR spectrometer equipped with a
289 Bruker IRscope II microscope and a MCT detector. Absorption spectra were collected in
290 the mid-infrared region (MIR) for quantification of H_2O and D_2O in synthetic FIs using a
291 globar light source and a KBr beamsplitter. Near-infrared (NIR) spectroscopy was applied
292 for measurement of water species in glasses using a tungsten light source and a CaF_2
293 beamsplitter. The spectral resolution was 2 cm^{-1} and 50 cans were accumulated in the MIR
294 region, 100 scans were measured with 4 cm^{-1} resolution in the NIR region.

The composition of silicate melt and cuprite pellets was determined on polished sections using an electron probe micro-analyzer (EMPA) CAMECA SX100. The reference materials for calibration included jadeite (Na), kyanite (Al), wollastonite (Si, Ca), orthoclase (K), NaCl (Cl) and Cu (Cu). Raw analytical data were corrected using the standard PAP procedure (Pouchou and Pichoir, 1991). Acceleration voltage was set as 15 kV. A focused beam and 15 nA beam current were used for cuprite analysis, and a slightly defocused beam (2 μm) and 5 nA beam current were used for Na-bearing silicate glass determination.

3. Results

3.1 Observations of quenched fluids

Precipitates were found in Cu capsules with ±Cu_2O±CuCl+HCl except for Cu +NaCl, and Cu+CuCl (DQ-47) (Table 1). In the case of DQ-42 and DQ-43 the precipitates were identified as CuCl by EDX analyses in a scanning electron microscopy. Both visual inspection of the capsule and the ICP-OES analyses of DQ-169 indicate that the added Cu_2O powder was fully consumed by the reaction with HCl, resulting in less acidic fluids (pH= 4.06) than the initial solution (pH= ~0). Quench fluids of runs containing initial HCl but no Cu_2O were still mild to very acidic after the run, suggesting that HCl has not completely reacted. For all NaCl-bearing experiments pH determination on quenched fluids indicate neutral to basic condition (Table 2). Solutions are also mild acidic when

only H_2O was loaded into Cu capsules (DQ-37A, B, C), probably because of formation of $Cu(OH)_2^-$ complexes via a reaction $Cu + 2\ H_2O = Cu(OH)_2^- + H^+ + ½\ H_2$.

3.2 Fluid inclusion microscopy

Results of microscopic investigation on sections of quartz cylinders are separately discussed for the systems ±Cu±Cu_2O+NaCl and Cu±CuCl±Cu_2O±HCl in the order of increasing quench rate, corresponding information is also tabulated in Table 1. Petrographic examination of quartz sections showed that the i.s. Qz had fewer and narrower cracks than the pref. Qz.

3.2.1 ±Cu±Cu_2O+NaCl system

Different observations were achieved depending on the copper source in these experiments. Only one type of inclusions was formed when Cu_2O was used, but two different types of inclusions were found in runs with metallic Cu. In experiments with Cu_2O (DQ-187, 188) typical FIs are visible containing a liquid phase, a vapor shrinkage bubble and daughter crystals (CuCl; Fig. 3a). The peculiarity of the experiments with Cu (DQ-21, 22, 23, 36, 121, 145, 146, 154, 165, 183) is the observation of silicate melt inclusions (SMIs) in addition to FIs. SMIs usually consisted of a vapor bubble, a liquid phase, sodium-bearing silicate glass and one or several reddish to dark opaque minerals. A carefully inspection of the capsule after Cu+NaCl runs indicated that there was not any silicate melt on the walls of the capsule. Thus, silicate melt was only formed in fractures of quartz and subsequent

333 healing of quartz produces the SMIs. Possible reason for this observation is lower surface
334 tension for the melt/quartz interface compared to melt/metal or fluid/melt interfaces.

335 Microthermometric determination demonstrates that the measured $NaCl_{eq.}$ values of
336 FIs of the Cu+NaCl system yield $NaCl_{eq.}$ values similar to the initial NaCl contents,
337 whereas this value was lower than the initial one in the Cu_2O+NaCl system (i.e., 6.8±0.1
338 wt% compared to the initial 8 wt% NaCl; Table 1). In the Cu+NaCl system we observe
339 that the homogenization temperature of FIs is 440-480°C, and the SMIs were not subject
340 to any visible change upon heating (up to 600°C) and freezing (down to -100°C). The
341 detailed inclusion petrography of the Cu+NaCl system is as follows.

342 [1] *SQ (DQ-21,22, 23)*: The size of most FIs varied from 20 to 30 μm. The relative
343 abundance of the SMIs is dependent on the initial NaCl content in the system. The SMIs
344 accounted for <5%, 10-15% and 30-40% of inclusions in 0.17, 1.49 and 4.28 m NaCl-
345 bearing runs, respectively. Note that percentage was estimated based on ca. 50 inclusions.
346 The shape of these inclusions changed from small isolated inclusion to large connected
347 channels with increasing salinity. In SQ experiment without $SiO_{2(gel)}$ inclusions tend to be
348 less abundant and smaller than those in runs with $SiO_{2(gel)}$. Nevertheless, both FIs and SMIs
349 were always found in both quartz chips. The sizes of inclusions were up to 20 μm (FI) and
350 up to 30 μm (SMI) in pref. Qz, whereas the i.s. Qz cylinder contained very few and tiny
351 inclusions, which made the interpretation of LA-ICP-MS data difficult.

352 [2] *SQ+RQ (DQ-145)*: Inclusions in pref. Qz were less abundant than in the *SQ* runs. The
353 size of FIs and SMIs was below 20 μm and 25 μm, respectively. SMIs usually contained
354 more cuprite crystals than FIs. Cuprite crystals were especially enriched in necking down
355 channels in SMIs. In contrast, few tiny inclusions were preserved in i.s. Qz.

356 [4] *CAQ (DQ-146)*: In pref. Qz, the number of preserved FIs was least in NaCl-bearing
357 systems, and these inclusions were smaller than 25 μm. Isolated SMIs were smaller than
358 10 μm and connected channels containing submicrometer-sized cuprite crystals were
359 common. Very few inclusions could be found in i.s. Qz.

360 [5] *RQ (DQ-183, 154, 165)*: Three runs with the same starting materials and cooling rate
361 but different run durations (2-14 d) were conducted. The number and size (15-30 μm) of
362 inclusions in pref. Qz of DQ-183 is comparable to the long runs (DQ-154 and DQ-165) but
363 only few inclusions (<10 μm) were found in the i.s. Qz of DQ-183, since no intermediate
364 quench was performed. Most FIs retrieved from these runs contained cuprite (Fig.3e),
365 while SMIs contained no discernible minerals and appeared to be rather homogeneous
366 (Fig.3f).

367 *3.2.2 Cu±CuCl±Cu_2O±HCl system*

368 Only one type of FIs was observed in this system, consisting of a liquid, a vapor
369 bubble and/or a colorless to dark tetrahedral crystal, probably nantokite (CuCl; Fig.3b).
370 The suspected nantokite crystal tended to decompose with exposure to an incident Raman
371 beam. Berry et al. (2006) undertook experiments with similar starting materials (native Cu

372 and KCl solution) as in our study and used XANES spectroscopy to identify a similar
373 tetrahedral mineral as nantokite (CuCl). They noted that this mineral is not stable at room
374 temperature as well as under laser beam.

375 [1] *SQ (DQ-42, 43, 47)*: FIs were generally smaller than 25 μm, with an elongated oval to
376 irregular shape. In SQ experiment without $SiO_{2(gel)}$ FIs were less abundant than in the runs
377 in the presence of $SiO_{2(gel)}$ and were often smaller than 10 μm in size.

378 [3] *VSQ+RQ (DQ-123)*: It is worth noting that more inclusions were observed in this
379 system when compared with the SQ and RQ runs (DQ-42, 43, 47, 102,169), however, the
380 total amount is far less than that produced in NaCl-bearing systems. The size of these
381 inclusions was smaller than 20 μm.

382 [5] *RQ (DQ-102, 169)*: This run contained the smallest amount of inclusions, which were
383 generally smaller than 20 μm. Nantokite could only be observed in the largest inclusions.
384 The inclusions retrieved from i.s. Qz were too small to be measured with LA-ICP-MS.

385 ***3.3 Chemical and spectroscopic analyses***

386 A polished quartz sections of DQ-21 was studied by EMPA and Raman spectroscopy.
387 Figure 4 shows a typical backscattered electron (BSE) image of a SMI. The EMPA total
388 of glasses in SMIs varies from 71 wt% to 91wt% (details are given in Table A2). These
389 low totals may originate from unmeasured H_2O but also from the small beam size needed
390 for measurements within the inclusions. Na_2O and Cu_2O contents of the glasses show high

391 variability but are generally low while SiO_2 is the predominant component in all analyses.
392 Atomic ratios up to 0.13 for Na/Si and up to 0.10 for Cu/Si are estimated from the data in
393 Table A2. Chlorine content was always very low (≤ 0.35 wt%). Analyses of the tiny
394 minerals include contributions of the glasses. Nevertheless, it is evident that these are
395 copper-rich minerals.

396 Raman spectra were recorded on the opaque minerals trapped in FIs and SMIs from
397 both *SQ* (DQ-21) and *RQ* (DQ-183) runs in the ±Cu±Cu_2O+NaCl systems. In addition to
398 bands of the host quartz, the Raman spectra of this opaque mineral exhibit five complex
399 bands, centered at 146, 218, 308, 412 and 625 cm^{-1} (Fig.5a), consistent with spectra of
400 natural cuprite (Database of Raman spectroscopy, X-ray diffraction and chemistry of
401 minerals (RRUFF), http://rruff.info/cuprite/ display=default/R050374). Cuprite (i.e. Cu_2O)
402 can be found in both types of inclusions while its abundance highly depends on the cooling
403 rate, i.e., it becomes more abundant in SMIs with decreasing rate, and in FIs with increasing
404 rate (see discussions).

405 Fig. 5b shows the Raman spectra of the silicate melt phase from these two runs. The
406 broad band system at 950-1100 cm^{-1} is attributed to Si-O stretching vibrations. Band
407 features resembles those of silicate glasses; the high wavenumbers indicate high degree of
408 polymerization (Colomban and Schreiber, 2005). Raman spectra of SMIs recorded over a
409 large wavenumber range of 50-4000 cm^{-1} give clear evidence for a pronounced peak at
410 3500 cm^{-1} (not shown here, but similar to the IR spectra in Fig.11a), indicating the presence

411 of H_2O in these SMIs. High water content is consistent with the low totals in the EMP
412 analysis.

413 ***3.4 LA-ICP-MS data standardization***

414 In this study we analyzed the content of five isotopes with masses of ^{23}Na, ^{28}Si, ^{65}Cu,
415 ^{85}Rb and ^{133}Cs in FIs with LA-ICP-MS (a typical example is shown in Fig. 2), and the
416 results are tabulated in Table 2. Using Rb and Cs, initially doped in solution as internal
417 standards to normalize LA-ICP-MS data, is widely accepted technique in synthetic FI
418 studies (e.g., Duc-Tin et al., 2007; Lerchbaumer and Audétat, 2012; Derrey et al., 2017).
419 When using Rb as internal standard, the obtained Na content is in good agreement with the
420 microthermometrically determined $NaCl_{eq.}$value in the Cu-free experiments with NaCl
421 solutions (DQ-99, 100, 101). On the other hand, the obtained Na content is slightly lower
422 than the $NaCl_{eq.}$value in the Cu_2O+NaCl system, which may be due to formation of $CuCl_2^-$
423 complexes which reduce the number of species in the fluid (Hack and Marvogenes, 2006).
424 But in the Cu+NaCl system, the evaluated Na content in FIs is not consistent with the
425 $NaCl_{eq.}$ value. An explanation is that Rb strongly partitions into the melt phase, and the Rb
426 content of the fluid is decreased (Fig.6). Therefore, the $NaCl_{eq.}$ value (as suggested by
427 Günther et al., 1998) is used for determination of element content in FIs of the Cu+NaCl
428 system whereas the initial Rb content is used to evaluate data of the Cu_2O+NaCl and Cu ±
429 CuCl± Cu_2O ± HCl systems, i.e. systems without SMIs.

3.5 Effect of run duration and intermediate quench on FIs

To understand the mechanism of FI formation, three experiments with the same starting materials (Cu+1.5 m NaCl) but different run durations were performed using the rapid quench technique (Table 1). As shown in Fig.1b, there are two stages during FI synthesis: (i) prior to intermediate quench (DQ-183) and (ii) after intermediate quench (i.s. Qz cylinders of DQ-154 and DQ-165).

Figure 7 depicts the variations of Cu, Rb and Cs as a function of run duration. It is evident that the short run (2 d; DQ-183) shows larger variation of element content than the long runs (8 and 14 d for DQ-154 and DQ-165, respectively). This may indicate that the reaction process is more complex than simple metallic Cu dissolution in fluid, and fluid-metal equilibration may need a long time. The Rb and Cs contents were not only much lower than their initial values but also had been decreasing with run durations, whereas the average Cu content increased with time. These trends imply that Rb and Cs is preferentially partitioned into the melt phase compared to Cu. Additionally, variations of Rb, Cs, and Cu content in i.s. Qz were smaller than those in pref. Qz indicating that fluid composition needs time for equilibration (a similar observation has been made by Derrey et al. (2017)).

3.6 Effect of silica gel on FIs

Figure 8 describes Cu variations relative to the Cs content of FIs in presence or absence of silica gel for Na^+ bearing and Na^+ free systems. It is apparent that the average Cu content

449 in DQ-43 (Cu+1.5 m HCl) is almost 8 times higher than that of DQ-21 (Cu+1.5 m NaCl).
450 In the presence of silica gel, rather constant Cs and Cu concentrations are achieved for both
451 pref. Qz and i.s. Qz cylinders in both systems. In the absence of silica gel, the variation of
452 Cs content is several times larger than in runs with addition of silica gel. These observations
453 clearly demonstrate the positive role of silica gel in healing of fractures and closing of
454 inclusions in quartz.

455 ***3.7 Cu content in fluid inclusions and quenched fluids***

456 In the experiments using Cu capsules filled with pure water (DQ-37A, B, C), the Cu
457 content of FIs (DQ-37A) is an order of magnitude lower than that of quenched fluid
458 extracted from DQ-37B, 37C (Table 2) although the run duration was much shorter for the
459 latter two experiments. This points to difficulties in using quenched fluids for solubility
460 determination. We suggest that this discrepancy can originate from contamination of the
461 fluid by Cu particles or clusters released from the capsule.

462 Large difference in Cu content of FIs and quenched fluids were also observed for runs
463 DQ-165 (1.5 m NaCl) and DQ-169 (1.5 m HCl). Here, the low Cu content in the quenched
464 fluid is due to precipitation of Cu-bearing species. Due to difficulties to completely extract
465 the precipitates from the capsule, we did not proceed with analyses on quenched fluids.

466 Fig.9 depicts that Cu content in the fluid is strongly enhanced by the availability of
467 chloride. (i) A nearly 1:1 ratio of Cu/Cl in FIs was derived from the measured Cu content

and initial chloride content for experiments in which HCl was added. And this ratio can be lowered by the addition of different monovalent Cu species. (ii) A Cu/Cl ratio of 1:9 was found in the fluid of Cu+NaCl system.

4. Discussion

4.1 Attainment of equilibrium between fluids and metals

Slow quench rates (~0.5 - ~0.8 K s^{-1}) were favored by most researchers to avoid inclusion decrepitation and to preserve more inclusions (Zhang et al., 2012; Derrey et al., 2017; Hack and Mavrogenes, 2006). In addition to slow quench, we applied various cooling rates to investigate their effects on Cu content of fluids trapped in inclusions (Table 1 and Fig. 10). A key observation is that the appearance of cuprite in both FI and SMI depends on the cooling rate (Fig. 10). In FIs, the presence of cuprite is mainly observed at fast cooling rate (Fig.10 d, f), but cuprite could not be discerned at slow cooling rates (Fig.10b). This may be due to the nucleation behavior of cuprite. During rapid cooling, cuprite is likely formed by homogeneous nucleation within the fluid (Fig.10f) while at intermediate quench cuprite is preferentially deposited on the inclusion wall by heterogeneous nucleation (Fig.10d). In SMIs, the presence of cuprite is mainly observed at slow-intermediate cooling rates (Fig. 10a, b), but not observed at fast cooling rates (Fig.10e). This observation is consistent with findings of Lowenstern (1995) that the degree of crystallization in melt inclusions positively correlates with cooling rate. The different

formation of cuprite in SMIs and FIs might be due to the higher viscosity of silicate melt compared to the fluid phase.

The observation of quench phases (cuprite, nantokite) in the inclusions makes it clear that the entire inclusions must be analyzed to draw conclusions about the Cu contents in fluids and melts. In the series of experiments with native and 1.5 m NaCl solution, the bulk copper content in FIs remains constant independent of cooling rates as well as presence of cuprite, averaging at ~0.16 m (Table 2). The standard error $\leq \pm 0.12$ m for the series is even lower than the typical standard error for FI analyses in a single quartz crystal (e.g., DQ-183, 43). The similarity of data of pref. and i.s. Qz imply that dissolution reaction of Cu is much faster than healing of quartz. However, the variation of Cu content in the SQ run (0.5 K s^{-1}) is about three times larger than that in the RQ run (25 K s^{-1}) (Fig. 10), which indicates that slowly cooled samples may be more affected by entrapment of FIs in the late state of cooling. Thus, rapid quench is a more effective technique to preserve information on the fluid at high T-P conditions at least in NaCl bearing systems. On the other hand, a clear disadvantage of RQ is the much smaller number of suitable FIs.

A crucial assumption in FI studies is that nothing is added to or removed from the inclusion following trapping (Roedder, 1984). However, several studies demonstrate that elements in inclusions can be mobilized in relatively short time at elevated temperatures and pressures (Mavrogenes and Bodnar, 1994; Audétat and Günther, 1999; Li et al., 2009; Audétat et al., 2018). The H_2O/D_2O exchange experiment (DQ-124) and Raman

spectroscopy show that single and isometric inclusions are well protected against exchange of fluid components, while large, irregularly shaped FIs remain open to the fluid and can easily exchange components (Fig. 11a, b). The duration of DQ-124 was one hour, i.e. much longer than the cooling time in most of our experiments. We therefore conclude that carefully selected FIs still reflect the state of the high-temperature fluids. A critical point in particular for studies on Cu solubility using the FI technique is that large amounts of Cu in inclusions can be gained or lost through diffusion in quartz, if Cu sources or sinks are available not too far away from the inclusion (e.g., Li et al., 2009; Lerchbaumer and Audétat, 2012; Rottier et al., 2017). The insensitivity of our data to quench rate is a strong argument that Cu diffusion in quartz did not significantly affect our experimental results. Therefore, the measured Cu content in FIs corresponds to at least near-equilibrium conditions of the system with respect to Cu solubility.

4.2 Cu solubility and Cu speciation in the fluid

The major focus of our study is on the interaction of precious copper with aqueous fluids. If the fluid consists of pure water, copper can be dissolved via the reaction

$$Cu_{(s)} + H_2O_{(fl)} = CuOH_{(fl)} + ½\ H_{2(fl)} \quad (1)$$

where subscripts (fl) and (s) refer to the fluid phase and to the solid phases, respectively. As pointed out by Zajacz et al. (2011) charged species are likely to be rather unstable in hydrothermal fluids at high temperature due to the low density and low dielectric constant

526 of the water. Thus, the dissolved copper species is probably $CuOH(H_2O)_x$, where x
527 signifies the number of H_2O molecules bond in a complex. The weak acidic behavior of
528 the quenched solution (pH=4) is consistent with such interpretation. Most likely,
529 dissociation of the copper complex according to the reaction

530 $$[CuOH(H_2O)_x]_{(l)} = [Cu(OH)_2(H_2O)_{x-1}]^-_{(l)} + H^+_{(l)} \qquad (2)$$

531 occurs in the liquid at low temperature, as signified here by the subscript (l). The average
532 Cu content of FIs of 0.004±0.002 m measured in run DQ-37A can be interpreted as Cu
533 solubility in pure water at 800°C, 200 MPa. The value is roughly consistent with the results
534 of Zajacz et al. (2011) who used gold capsules alloyed with 3% Cu to adjust a copper
535 activity of 0.01 and found the Cu content in the fluid to be <0.0001 m at 1050°C, 150 MPa.
536 However, direct comparison of the data is not possible because of different P, T conditions.
537 Furthermore, hydrogen fugacity (f_{H2}) was much higher in their experiments (initial f_{H2} ≈19
538 bar) than in our experiments (f_{H2} ≈0.8 bar, Berndt et al. 2001). According to Eqn. (1) an
539 inverse square root dependence of Cu solubility on hydrogen fugacity is expected.

540 Copper solubility in hydrous fluids is strongly enhanced by complexation with
541 chlorine, e.g. by a factor of 40 when the solution contains 1.5 mol NaCl per kg. Concerning
542 the supply of chlorine, we need to distinguish two systems: (i) Chlorine is charge
543 compensated by alkali and (ii) alkalis are absent and chlorine is added as HCl or CuCl.
544 Both scenarios are discussed in following.

545 4.2.1. Copper solubility in NaCl-bearing solutions

546 The first step of copper dissolution is the same as in Eqn. (1). Subsequently, OH^- is
547 substituted by Cl^- via the exchange reaction

548 $$CuOH_{(fl)} + NaCl_{(fl)} = CuCl_{(fl)} + NaOH_{(fl)} \quad (3)$$

549 Driving force is the much higher stability of copper chlorine complexes compared to
550 copper-hydroxide complexes. The high Cl/Cu ratio in the fluid observed in our study and
551 in previous studies (9:1 at a_{Cu} of 1, this study; 6:1 at a_{Cu} of 1, Berry et al. (2006); 200:1 at
552 a_{Cu} of 0.01, Zajacz et al. (2011)) supports formation of copper complexes with more than
553 1 Cl^- as ligand. Quantum chemical calculations of Zajacz et al (2011) also demonstrated
554 the high stability of species like $NaCuCl_2$ in the fluid. This can be described by the reaction

555 $$CuCl_{(fl)} + NaCl_{(fl)} = NaCuCl_{2(fl)} \quad (4)$$

556 NaOH can react with dissolved silica according to Anderson and Burham (1967) via

557 $$NaOH_{(fl)} + H_4SiO_{4(fl)} = NaH_3SiO_{4(fl)} + H_2O_{(fl)} \quad (5)$$

558 The overall reaction can be described by (Zajacz et al (2011)

559 $$Cu_{(s)} + SiO_{2(s)} + 2\ NaCl_{(fl)} + 2\ H_2O_{(fl)} = NaCuCl_{2(fl)} + NaH_3SiO_{4(fl)} + ½\ H_{2(fl)} \quad (6)$$

560 In our experiments the Cu activity was much higher than in the study of Zajacz et al.
561 (2011) and, hence, the concentration of dissolved Cu as well as dissolved silica was much
562 higher. The higher degree of reaction explains the formation of SMIs in our study. The

563 co-appearance of FIs and SMIs in quartz implies that the system is at least close to liquid
564 immiscibility. However, based on our experiments it cannot be approved that silica-rich
565 melt and H_2O-rich fluid represent equilibrium conditions of the system. The fact that
566 silicate melts are found only within (former) cracks and that the composition of SMIs
567 within a single quartz chip show large variability suggest that reaction kinetics and
568 transport within fractures play an important role. Furthermore, one needs to be aware that
569 inclusions may have been trapped at different stages during the experiment.

570 4.2.1. Copper mobility in alkali-free Cl-bearing systems

571 If HCl is added to metallic copper, high amount of hydrogen is produced insight the
572 capsule through the reaction

573 $$Cu_{(s)} + HCl_{(fl)} = CuCl_{(fl)} + H_{2(fl)} \quad (7)$$

574 but permeation of hydrogen through capsule is fast enough to equilibrate hydrogen fugacity
575 in the capsule interior with the pressure medium within an hour (Reiter et al. 1993). Thus,
576 the state recorded in the FIs corresponds to a hydrogen fugacity of ~0.8 bar. The 1:1 ratio
577 of Cl/Cu measured in experiments with various initial concentrations of HCl implies that
578 reaction (7) completely proceeds to the right side. However, the post-experimental
579 solutions are moderate to very acidic, suggesting that some unreacted HCl is still present.
580 It is noteworthy that the low acidity of aqueous solutions at room temperature is supported
581 by high density of the solvent and dissociation of HCl. In high temperature fluid, HCl is

582 most likely present as a neutral molecule (Zajacz et al. 2011). The high acidity of the
583 solution after the experiment with Cu + CuCl (pH=1, DQ-47) indicates some back reaction
584 of (7) with formation of HCl and metallic copper. At our run conditions excess HCl is most
585 likely bonded to a copper complex via

586 $$CuCl_{(fl)} + HCl_{(fl)} = HCuCl_{2(fl)} \quad (8)$$

587 Quantum chemical calculations of Zajacz et al. (2011) confirm the stability of $HCuCl_2$
588 complexes in high temperature fluids.

589 A key question is whether the whole amount of CuCl produced by reaction (7) can be
590 re-dissolved in the fluid or not? Massive nantokite was observed in the quenched fluid even
591 at the lowest HCl content (0.5 m HCl; DQ-123), and the copper content detected in FIs is
592 much higher than that in any experiments with NaCl. On the other hand, the stability of
593 $NaCuCl_2$ complexes in aqueous fluids is much higher than for $HCuCl_2$ complexes (Zajacz
594 et al. 2011). Thus, it is very likely that the solubility of CuCl has been exceeded in the
595 experiments with HCl, and nantokite which was observed in FIs is a stable phase at the
596 experimental conditions. The analyses of FIs do not represent solubility of copper, but are
597 highly affected by contributions of the coexisting mineral nantokite.

598 **5. Implications**

599 Among the Cu-bearing deposits, porphyry copper deposits are of great importance as
600 they supply 75% of the world's copper (Sillitoe, 2010). These deposits are spatially linked

601 to magmatic systems, and exsolution of metal-bearing fluids from silicate melt without
602 sulfide saturation is believed to be efficient to form large porphyry Cu deposits (e.g., Cline
603 and Bodnar, 1991; Hedenquist and Richards,1998; Audétat and Simon, 2012). Furthermore,
604 coexistence of fluids and silicate melts (co-trapping of FIs and SMIs) can play a vital role
605 in Cu mobility. For instance, fluid inclusions containing weight percent of Cu (~10 wt%)
606 have been found to coexist with SMI in Bajo de la Alumbrera porphyry Cu-Au deposit
607 (Harris et al., 2003). Likewise, coeval SMIs and FIs have also been documented elsewhere,
608 such as in the Río Blanco Cu-Mo deposit (Davidson and Kamenetsky, 2007), Elatsite
609 porphyry Cu-Au deposit (Stefanova et al., 2014), Cerro de Pasco porphyry-type deposit
610 (Rottier et al., 2016), and the Grasberg porphyry Cu-Au deposit (Mernagh and Mavrogenes,
611 2018). However, our experiments have demonstrated that silicate-rich liquids can be also
612 formed in initially water-dominated quartz bearing hydrothermal systems. It seems that
613 melt generation requires basic solutions and formation of hydroxide- and Si-bearing
614 complexes. This finding may have important implications for the transport of fluids, liquids
615 and metals in the magmatic-hydrothermal systems, although additional studies are required
616 to better understand the nature of such thermosilicate liquids, in particular, the kinetics and
617 mechanism(s) of their formation.

618 The stability of cuprite (Cu_2O), nantokite (CuCl) and occurrence of metallic Cu in
619 some of our experiments indicate that these Cu species can play a significant role in the
620 formation of Cu deposits in the systems with low S activity. One of the unique examples

621 is the ore deposits of the Keweenaw Peninsula, where native copper accounts for more than
622 99% of the district's production (ca. 5 billion kg of refined copper) in the period of 1845-
623 1968 (Weege and Pollack, 1971). Bornhorst and Mathur (2017) proposed that the sulfur-
624 poor Keweenaw basalt was enriched in Cu (e.g., native copper) and underwent later burial
625 metamorphism; the progressive batches of metamorphogenic ore-forming fluids with
626 similar copper isotopic compositions of the source rock transported Cu as Cu^+ (e.g. $CuCl_2^-$).
627 The final reductive precipitation of native copper from metamorphogenic ore-forming
628 fluids was facilitated by mixing with meteoric waters. The data obtained in this study
629 indicate that the precipitation of native Cu may happen also at high temperature and high
630 pressure. The precipitation of native Cu from Cu^+-bearing hydrothermal fluids may occur
631 when the fluid is less acidic (i.e., H^+ is absent) and the process can be initiated under
632 reduced conditions.

633 **Acknowledgments**

634 This research was supported by the German Academic Exchange Service (DAAD-
635 57076462) and Graduate School GeoFluxes. We thank Moritz Albrecht, Martin Oeser-
636 Rabe, Ulrich Kroll and Julian Feige for their technical supports. We would also like to
637 thank Hongwu Xu and Kyle Ashley for editorial handling as well as two reviewers (Adam
638 Simon and Ryan Mathur) for their constructive and thorough comments on this manuscript.

References:

Albrecht, M., Derrey, I.T., Horn, I., Schuth, S. and Weyer, S. (2014). Quantification of trace element contents in frozen fluid inclusions by UV-fs-LA-ICP-MS analysis. Journal of Analytical Atomic Spectrometry, 29(6): 1034-1041. DOI: 10.1039/c4ja00015c.

Anderson, G. and Burham, C. (1967). Reactions of quartz and corundum with aqueous chloride and hydroxide solutions at high temperatures and pressures. Am. J. Sci.;(United States), 265(1): 12-27. DOI: 10.2475/ajs.265.1.12.

Archibald, S., Migdisov, A.A. and Williams-Jones, A. (2001). The stability of Au-chloride complexes in water vapor at elevated temperatures and pressures. Geochimica et cosmochimica acta, 65(23): 4413-4423. DOI: 10.1016/S0016-7037(01)00730-X.

Archibald, S., Migdisov, A.A. and Williams-Jones, A. (2002). An experimental study of the stability of copper chloride complexes in water vapor at elevated temperatures and pressures. Geochimica et cosmochimica acta, 66(9): 1611-1619. DOI: 10.1016/S0016-7037(01)00867-5.

Audétat, A. and Günther, D. (1999). Mobility and H_2O loss from fluid inclusions in natural quartz crystals. Contributions to Mineralogy and Petrology, 137(1-2): 1-14. DOI: 10.1007/s004100050578.

Audétat A, Simon AC (2012) Magmatic Controls on Porphyry Copper Genesis. SEG Spec Publ 16:553–572

Audétat, A., Zhang, L. and Ni, H. (2018). Copper and Li diffusion in plagioclase, pyroxenes, olivine and apatite, and consequences for the composition of melt inclusions. Geochimica et Cosmochimica Acta DOI: 10.1016/j.gca.2018.09.016.

Bakker, R.J. (2003). Package FLUIDS 1. Computer programs for analysis of fluid inclusion data and for modelling bulk fluid properties. Chemical Geology, 194(1): 3-23. DOI: 10.1016/S0009-2541(02)00268-1.

Berndt, J., Holtz, F. and Koepke, J. (2001). Experimental constraints on storage conditions in the chemically zoned phonolitic magma chamber of the Laacher See volcano. Contributions to Mineralogy and Petrology, 140(4): 469-486. DOI: 10.1007/Pl00007674.

Berry, A.J., Hack, A.C., Mavrogenes, J.A., Newville, M. and Sutton, S.R. (2006). AXANES study of Cu speciation in high-temperature brines using synthetic fluid inclusions. American Mineralogist, 91(11-12): 1773-1782. DOI: 10.2138/am.2006.1940.

Bodnar, R., Lecumberi-Sanches, P., Moncada, D. and Steele-MacInnis, M. (2014). Fluid inclusions in hydrothermal ore deposits, Treatise on Geochemistry 2nd Edition, pp. 119-142.

Bodnar, R. and Sterner, S. (1987). Synthetic Fluid Inclusions, in"Hydrothermal Experimental Techniques", Barnes, HL, Ulmer, GC, cds. Wiley and Sons, New York.

Bornhorst, T.J. and Mathur, R. (2017). Copper Isotope Constraints on the Genesis of the Keweenaw Peninsula Native Copper District, Michigan, USA. Minerals, 7(10): 185. DOI: 10.3390/min7100185.

Brugger, J., Etschmann, B., Liu, W., Testemale, D., Hazemann, J.L., Emerich, H., van Beek, W. and Proux, O. (2007). An XAS study of the structure and thermodynamics of Cu (I) chloride complexes in brines up to high temperature (400°C, 600 bar). Geochimica et cosmochimica acta, 71(20): 4920-4941. DOI: 10.1016/j.gca.2007.08.003.

Brugger, J., McPhail, D., Black, J. and Spiccia, L. (2001). Complexation of metal ions in brines: application of electronic spectroscopy in the study of the Cu (II)-LiCl-H_2O system between 25 and 90°C. Geochimica et Cosmochimica Acta, 65(16): 2691-2708. DOI: 10.1016/S0016-7037(01)00614-7.

Butler, B.S. and Burbank, W.S. (1929). The copper deposits of Michigan. US Government Printing Office.

Candela, P.A., Holland, H.D. (1984). The partitioning of copper and molybdenum between silicate melts and aqueous fluids. Geochim Cosmochim Acta 48:373–380. doi: 10.1016/0016-7037(84)90257-6

Cline, J.S., Bodnar, R.J. (1991). Can economic porphyry copper mineralization be generated by a typical calc-alkaline melt? J. Geophys. Res. 96, 8113–8126. https://doi.org/10.1029/91JB00053

Colomban, P. and Schreiber, D.H. (2005). Rman signature modification induced by copper nanoparticles in silicate glass. Journal of Raman Spectroscopy, 36: 884-890. DOI: 10.1002/jrs.1379

Crerar, D.A. and Barnes, H. (1976). Ore solution chemistry; V, Solubilities of chalcopyrite and chalcocite assemblages in hydrothermal solution at 200 degrees to 350 degrees C. Economic Geology, 71(4): 772-794. DOI: 10.2113/gsecongeo.71.4.772.

Davidson, P., Kamenetsky, V.S., 2007. Primary aqueous fluids in rhyolitic magmas: Melt inclusion evidence for pre- and post-trapping exsolution. Chem. Geol. 237, 372–383. https://doi.org/10.1016/j.chemgeo.2006.07.009

Derrey, I.T. Albrecht, M., Dupliy, E., Botcharnikov, R. E., Horn, I., Junge, M., Weyer, S. and Holtz, F. (2017). Experimental tests on achieving equilibrium in synthetic fluid inclusions: Results for scheelite, molybdenite, and gold solubility at 800 C and 200 MPa. American Mineralogist, 102(2): 275-283. DOI: 10.2138/am-2017-5869.

Duc-Tin, Q., Audétat, A. and Keppler, H. (2007). Solubility of tin in (Cl, F)-bearing aqueous fluids at 700 degrees C, 140 MPa: A LA-ICP-MS study on synthetic fluid inclusions. Geochimica Et Cosmochimica Acta, 71(13): 3323-3335. DOI: 10.1016/j.gca.2007.04.022.

Fulton, J.L., Hoffmann, M.M. and Darab, J.G. (2000). An X-ray absorption fine structure study of copper (I) chloride coordination structure in water up to 325°C. Chemical Physics Letters, 330(3): 300-308. DOI: 10.1016/S0009-2614(00)01110-6.

Guillong, M. and Heinrich, C.A. (2007). Sensitivity enhancement in laser ablation ICP-MS using small amounts of hydrogen in the carrier gas. Journal of Analytical Atomic Spectrometry, 22(12): 1488-1494. DOI: 10.1039/b709489b.

Guillong, M., Meier, D.L., Allan, M.M., Heinrich, C.A. and Yardley, B.W. (2008). Appendix A6: SILLS: A MATLAB-based program for the reduction of laser ablation ICP-MS data of homogeneous materials and inclusions. Mineralogical Association of Canada Short Course Series, 40: 328-333.

Günther, D., Audétat, A., Frischknecht, R. and Heinrich, C.A. (1998). Quantitative analysis of major, minor and trace elements in fluid inclusions using laser ablation–inductively coupled plasmamass spectrometry. Journal of Analytical Atomic Spectrometry, 13(4): 263-270. DOI: 10.1039/A707372K.

Hack, A.C.and Mavrogenes, J.A. (2006). A synthetic fluid inclusion study of copper solubility in hydrothermal brines from 525 to 725°C and 0.3 to 1.7 GPa. Geochimica et cosmochimica acta, 70(15): 3970-3985. DOI: 10.1016/j.gca.2006.04.035.

Harris, A.C., Kamenetsky, V.S., White, N.C., et al. (2003) Melt Inclusions in Veins: Linking Magmas and Porphyry Cu Deposits. Science (80-) 302:2109–2111. doi: 10.1126/science.1089927

Hedenquist, J. and Richards, J. (1998). The influence of geochemical techniques on the development of genetic models for porphyry copper deposits. Reviews in Economic Geology, 10(10): 235-256. DOI: 10.5382/Rev.10.10.

Holzheid, A. and Lodders, K. (2001). Solubility of copper in silicate melts as function of oxygen and sulfur fugacities, temperature, and silicate composition. Geochimica et cosmochimica acta, 65(12): 1933-1951. DOI: 10.1016/S0016-7037(01)00545-2.

Ikehata, K., Chida, K., Tsunogae, T. and Bornhorst, T.J. (2016). Hydrothermal Native copper in ocean island alkali basalt from the Mineoka Belt, Boso Peninsula, Central Japan. Economic Geology, 111(3): 783-794. DOI: 10.2113/econgeo.111.3.783.

Ikehata, K. and Hirata, T. (2012). Copper isotope characteristics of copper-rich minerals from the Horoman peridotite complex, Hokkaido, northern Japan. Economic Geology, 107(7): 1489-1497. DOI: 10.2113/econgeo.107.7.1489.

Jochum, K.P. Nohl, L., Herwig, K., Lammel, E., Toll, B. and Hofmann, A. W. (2005). GeoReM: a new geochemical database for reference materials and isotopic standards. Geostandards and Geoanalytical Research, 29(3): 333-338. DOI: 10.1111/j.1751-908X.2005.tb00904.x.

Lerchbaumer, L. and Audétat, A. (2012). High Cu concentrations in vapor-type fluid inclusions: An artifact? Geochimica Et Cosmochimica Acta, 88: 255-274. DOI: 10.1016/j.gca.2012.04.033.

Li, Y. and Audétat, A. (2009). A method to synthesize large fluid inclusions in quartz at controlled times and under unfavorable growth conditions. American Mineralogist, 94(2-3): 367-371. DOI: 10.2138/am.2009.3054.

Li, Y., Audétat, A., Lerchbaumer, L. and Xiong, X. (2009). Rapid Na, Cu exchange between synthetic fluid inclusions and external aqueous solutions: evidence from LA-ICP-MS analysis. Geofluids, 9(4): 321-329. DOI: 10.1111/j.1468-8123.2009.00255.x.

Liu, W., Brugger, J., Etschmann, B., Testemale, D. and Hazemann, J.-L. (2008). The solubility of nantokite (CuCl (s)) and Cu speciation in low-density fluids near the critical isochore: An in-situ XAS study. Geochimica et Cosmochimica Acta, 72(16): 4094-4106. DOI: 10.1016/j.gca.2008.05.056.

Liu, W., Brugger, J., McPhail, D. and Spiccia, L. (2002). A spectrophotometric study of aqueous copper (I)–chloride complexes in LiCl solutions between 100 C and 250°C. Geochimica et Cosmochimica Acta, 66(20): 3615-3633. DOI: 10.1016/S0016-7037(02)00942-0.

Liu, W. and McPhail, D. (2005). Thermodynamic properties of copper chloride complexes and copper transport in magmatic-hydrothermal solutions. Chemical Geology, 221(1): 21-39. DOI: 10.1016/j.chemgeo.2005.04.00.

Liu, W., McPhail, D. and Brugger, J. (2001). An experimental study of copper (I)-chloride and copper (I)-acetate complexing in hydrothermal solutions between 50 C and 250°C and vapor-saturated pressure. Geochimica et Cosmochimica Acta, 65(17): 2937-2948. DOI: 10.1016/S0016-7037(01)00631-7.

Lowenstern, J.B. (1995). Applications of silicate-melt inclusions to the study of magmatic volatiles. Magmas, Fluids Ore Depos. Mineral. Assoc. Canada Short Course 23, 71–99.

Matthews, W., Linnen, R.L. and Guo, Q. (2003). A filler-rod technique for controlling redox conditions in cold-seal pressure vessels. American Mineralogist, 88(4): 701-707. DOI: 10.2138/am-2003-0424.

Mavrogenes, J. and Bodnar, R. (1994). Hydrogen movement into and out of fluid inclusions in quartz: experimental evidence and geologic implications. Geochimica et Cosmochimica Acta, 58(1): 141-148. DOI: 10.1016/0016-7037(94)90452-9.

Mernagh, T.P. and Mavrogenes, J. (2018). Significance of high temperature fluids and melts in the Grasberg porphyry copper-gold deposit. Chemical Geology. DOI: 10.1016/j.chemgeo.2018.09.040.

Mountain, B. and Seward, T. (1999). The hydrosulphide/sulphide complexes of copper (I): Experimental determination of stoichiometry and stability at 22°C and reassessment of high temperature data. Geochimica et Cosmochimica Acta, 63(1): 11-29. DOI: 10.1016/S0016-7037(98)00288-9.

Mountain, B. and Seward, T. (2003). Hydrosulfide/sulfide complexes of copper (I): experimental confirmation of the stoichiometry and stability of Cu $(HS)_2^-$ to elevated temperatures. Geochimica et cosmochimica acta, 67(16): 3005-3014. DOI: 10.1016/S0016-7037(03)00303-X.

Nagle, F., Fink, L., Boström, K. and Stipp, J. (1973). Copper in pillow basalts from La Désirade, Lesser Antilles island arc. Earth and Planetary Science Letters, 19(2): 193-197. DOI: 10.1016/0012-821X(73)90114-3.

760 Nash, J.T. (1976). Fluid-inclusion petrology--data from porphyry copper deposits and applications to exploration: a
761 summary of new and published descriptions of fluid inclusions from 36 porphyry copper deposits and discussion of
762 possible applications to exploration for copper deposits. US Govt. Print. Off.
763 Neumann, J., Zhong, T. and Chang, Y. (1984). The Cu−O (Copper-Oxygen) system. Journal of Phase Equilibria, 5(2):
764 136-140. DOI: 10.1007/BF02868948.
765 Pinto, V.M., Hartmann, L.A. and Wildner, W. (2011). Epigenetic hydrothermal origin of native copper and supergene
766 enrichment in the Vista Alegre district, Paraná basaltic province, southernmost Brazil. International Geology
767 Review, 53(10): 1163-1179. DOI: 10.1080/00206810903464547.
768 Pitzer, K.S. and Sterner, S.M. (1994). Equations of state valid continuously from zero to extreme pressures for H_2O and
769 CO_2. The Journal of chemical physics, 101(4): 3111-3116. DOI: 10.1063/1.467624.
770 Pouchou, J. L. and Pichoir, F. (1991). Quantitative analysis of homogeneous or stratified microvolumes applying the
771 model "PAP", Electron probe quantitation. Springer, pp. 31-75.
772 Reiter, F., Forcey, K. and Gervasini, G. (1993). A compilation of tritium-material interaction parameters in fusion
773 reactor materials. Commission of the European Communities.
774 Rempel, K.U., Liebscher, A., Meixner, A., Romer, R.L. and Heinrich, W. (2012). An experimental study of the
775 elemental and isotopic fractionation of copper between aqueous vapour and liquid to 450° C and 400 bar in the
776 CuCl–NaCl–H_2O and CuCl–NaHS–NaCl–H_2O systems. Geochimica et Cosmochimica Acta, 94: 199-216. DOI:
777 10.1016/j.gca.2012.06.028.
778 Ripley, E.M. and Brophy, J.G. (1995). Solubility of copper in a sulfur-free mafic melt. Geochimica et cosmochimica
779 acta, 59(23): 5027-5030. DOI: 10.1016/0016-7037(95)00387-8.
780 Roedder, E. (1984). Fluid Inclusions. Fluid Inclusions.
781 Rottier, B., Kouzmanov, K., Bouvier, A.S., Baumgartner, L.P., Wälle, M., Rezeau, H., Bendezú, R., Fontboté, L. (2016).
782 Heterogeneous melt and hypersaline liquid inclusions in shallow porphyry type mineralization as markers of the
783 magmatic-hydrothermal transition (Cerro de Pasco district, Peru). Chem. Geol. 447, 93–116.
784 https://doi.org/10.1016/j.chemgeo.2016.10.032
785 Rottier, B. Rezeau, H., Casanova, V., Kouzmanov, K., Moritz, R., Schlöglova, K., Wälle, M. and Fontboté, L. (2017).
786 Trace element diffusion and incorporation in quartz during heating experiments. Contributions to Mineralogy and
787 Petrology, 172(4): 23. DOI: 10.1007/s00410-017-1350-4.
788 Schmidt, C., Watenphul, A., Jahn, S., Schäpan, I., Scholten, L., Newville, M, G. and Lanzirotti, A. (2018). Copper
789 complexation and solubility in high-temperature hydrothermal fluids: A combined study by Raman, X-ray
790 fluorescence, and X-ray absorption spectroscopies and ab initio molecular dynamics simulations. Chemical Geology,
791 494: 69-79. DOI: 10.1016/j.chemgeo.2018.07.018.
792 Seward, T. and Barnes, H. (1997). Metal transport by hydrothermal ore fluids. Geochemistry of hydrothermal ore
793 deposits: 435-486.
794 Sherman, D.M. (2007). Complexation of Cu+ in hydrothermal NaCl brines: ab initio molecular dynamics and energetics.
795 Geochimica et Cosmochimica Acta, 71(3): 714-722. DOI: 10.1016/j.gca.2006.09.015.
796 Sillitoe, R.H. (2010) Porphyry copper systems. Economic Geology 105, 3-41.
797 Stefanova, E., Driesner, T., Zajacz, Z., Heinrich, C.A., Petrov, P., Vasilev, Z. (2014). Melt and fluid inclusions in
798 hydrothermal veins: The magmatic to hydrothermal evolution of the elatsite porphyry Cu-Au deposit, Bulgaria.
799 Econ. Geol. 109, 1359–1381. https://doi.org/10.2113/econgeo.109.5.1359
800 Stoiber, R.E. and Davidson, E.S. (1959). Amygdule mineral zoning in the Portage Lake lava series, Michigan copper
801 district; Part II. Economic Geology, 54(8): 1444-1460. DOI: 10.2113/gsecongeo.54.7.1250.
802 Swamy, V., Saxena, S.K., Sundman, B. and Zhang, J. (1994). A thermodynamic assessment of silica phase diagram.
803 Journal of Geophysical research-all series, 99: 11,787-11,787. DOI: 10.1029/93JB02968.
804 Thompson, R.A. and Helz, G.R. (1994). Copper speciation in sulfidic solutions at low sulfur activity: Further evidence
805 for cluster complexes? Geochimica et Cosmochimica Acta, 58(14): 2971-2983. DOI: 10.1016/0016-
806 7037(94)90172-4.
807 Var'yash, L. (1992). Cu (I) complexing in NaCl solutions at 300 and 350 C. Geochem. Int, 29(3): 84-92.
808 Wang, C.Y.,Zhou, M.F., Qi, L., Hou, S., Gao, H., Zhang Z., Malpas J., 2006. The Zhaotong native copper deposit
809 associated with the Permian Emeishan flood basalts, Yunnan, Southwest China. International Geology Review,
810 48(8): 742-753. DOI: 10.2747/0020-6814.48.8.742.
811 Weege, R. and Pollack, J. (1971). Recent developments in the native-copper district of Michigan, Society of Economic
812 Geologists Guidebook for Field Conference, Michigan Copper District, pp. 18-43.
813 Williams-Jones, A.E., Migdisov, A.A., Archibald, S.M. and Xiao, Z. (2002). Vapor-transport of ore metals. Water–
814 Rock Interaction, Ore Deposits, and Environmental Geochemistry: A Tribute to David A. Crerar: 279-306.
815 Xiao, Z., Gammons, C. and Williams-Jones, A. (1998). Experimental study of copper (I) chloride complexing in
816 hydrothermal solutions at 40 to 300 C and saturated water vapor pressure. Geochimica et cosmochimica acta, 62(17):
817 2949-2964. DOI: 10.1016/S0016-7037(98)00228-2.
818 Zajacz, Z., Candela, P.A., Piccoli, P.M., Wälle, M. and Sanchez-Valle, C. (2012). Gold and copper in volatile saturated
819 mafic to intermediate magmas: Solubilities, partitioning, and implications for ore deposit formation. Geochim.
820 Cosmochim. Acta 91, 140–159. https://doi.org/10.1016/j.gca.2012.05.033

Zajacz, Z., Seo, J.H., Candela, P.A., Piccoli, P.M. and Tossell, J.A. (2011). The solubility of copper in high-temperature magmatic vapors: a quest for the significance of various chloride and sulfide complexes. Geochimica et cosmochimica acta, 75(10): 2811-2827. DOI: 10.1016/j.gca.2011.02.029.

Zhang, D., Zhou, T., Yuan, F., Fiorentini, M.L., Said, N., Lu, Y. and Pirajno, F. (2013). Geochemical and isotopic constraints on the genesis of the Jueluotage native copper mineralized basalt, Eastern Tianshan, Northwest China. Journal of Asian Earth Sciences, 73: 317-333. DOI: 10.1016/j.jseaes.2013.04.043.

Zhang, L., Audétat, A. and Dolejš, D. (2012). Solubility of molybdenite (MoS2) in aqueous fluids at 600–800°C, 200MPa: A synthetic fluid inclusion study. Geochimica et cosmochimica acta, 77: 175-185. DOI: 10.1016/j.gca.2011.11.015.

Zhang, Y., Xu, Z. and Behrens, H. (2000). Hydrous species geospeedometer in rhyolite: improved calibration and application. Geochimica et Cosmochimica Acta, 64(19): 3347-3355. DOI: 10.1016/S0016-7037(00)00424-5.

Zhang, Z., Mao, J., Wang, F. and Pirajno, F. (2006). Native gold and native copper grains enclosed by olivine phenocrysts in a picrite lava of the Emeishan large igneous province, SW China. American Mineralogist, 91(7): 1178-1183. DOI: 10.2138/am.2006.1888.

Zhu, B., Hu, Y., Zhang, Z., Chang, X. (2003). Discovery of the copper deposits with features of the Keweenawan type in the border area of Yunnan and Guizhou provinces. Science in China Series D: Earth Sciences, 46(1): 60-72.

838 **List of table captions**

839 Table 1 Experimental design of fluid inclusion synthesis

840 Table 2 The composition of the fluid phase in the conducted experiments

841 Table A1 Initial loading of all runs

842 Table A2 EMP analyses of quartz and SMIs in run DQ-21 (in wt%)

843 **List of figure captions**

844 Figure 1 Schematic drawing of the experiment conducted in RH/RQ Ar-CSPV. (a) The
845 design of capsule, which is modified after Derrey et al. (2017); (b) Thermal history of the
846 experiment. The cooling rates were calculated based on the total time needed for the
847 temperature dropping from 800°C to 300°C at the external thermocouple.

848 Fig.2 Typical LA-ICP-MS signals of small (a) and large (b) frozen FIs using a UV-fs-laser,
849 heating-freezing cell and *Element XR* ICP-MS. (a) Small FI has been ablated by spot
850 ablation pattern. DQ21: Cu+$SiO_{2(gel)}$+1.49 m $NaCl_{aq}$. (b) Large FI has been ablated by
851 spiral ablation pattern. DQ36: Cu+1.49 m $NaCl_{aq}$.

852 Figure 3 Photomicrographs of typical quartz-hosted inclusions at 25°C. (a) Nantokite was
853 observed in FIs of the run with cuprite (Cu_2O) and NaCl solution (DQ-187); (b) Potential
854 nantokite was precipitated in FIs of the run with native Cu and HCl solution (DQ-43). (c,
855 d) Photos are taken from different area of the pref. Qz of DQ-21 in which FI (marked in
856 (c)) coexists with SMI (marked in (d)). Discernible cuprite crystals are observed in SMI in

857 despite of FI. (e, f) Both FI and SMI occur in the pref. Qz of DQ-183, no intermediate
858 quench was adopted. FI often contains cuprite aggregates.
859

860 Figure 4 A BSE image of a SMI in pref. Qz of DQ-21. The rounded bright dots were
861 identified as cuprite using Raman spectroscopy (see Fig. 5a).

862 Figure 5 Raman spectra of different phases in inclusions after SQ (DQ-21) and RQ (DQ-
863 183) runs. (a) Raman analyses of crystals trapped in FIs (DQ-183) and SMIs (DQ-21) in
864 comparison with natural cuprite and quartz host. The vertical dashed lines are assigned to
865 typical cuprite Raman bands (for more details in text). (b) Raman analyses of silicate melt
866 phase in comparison to quartz and FI. Broad bands at 550-600 cm^{-1} and 1000-1100 cm^{-1}
867 may be assigned to amorphous silica (see text). *SQ* and *RQ* refer to runs and, respectively.

868 Figure 6 Examples of Na contents in FIs based on the internal standard Rb (400 $\mu g\ g^{-1}$).
869 The gray bar represents $Na_{eq.}$ which is evaluated Na content from microthermometry
870 measurement; $Na_{initial}$ denotes the initial Na content estimated from the starting solution.

871 Figure 7 Average Cu, Rb and Cs concentrations of FIs (error bar is given by the standard
872 deviation of the data). All runs were conducted with same material and same condition
873 using rapid quench technique. Intermediate quench was performed after 0 (DQ-183), 2
874 (DQ-154) and 4 (DQ-165) d.

875 Figure 8 Cu content versus Cs content in Na^+ bearing and Na^+ free runs using SQ technique.

Figure 9 Cu concentrations as a function of initial chloride concentration in Cu±Cu_2O±CuCl±NaCl±HCl systems. All runs were performed in Cu capsules with cooling rate of 0.5 K s^{-1}, except for the run with Cu_2O+NaCl (Au capsule). Red symbols represent the runs with NaCl solution, whereas other symbols stand for the runs with Na-free solution. Solid line is a regression relation between the average Cu concentration derived from Cu+NaCl system and initial chloride concentration. Dashed line represents Cu/Cl ratio of 1:1.

Figure 10 Cu content of FIs as a function of cooling rate, and the presence of cuprite in FIs and SMIs with respect to cooling rate. All runs were conducted in Cu+1.49 m NaCl system. (a, b) DQ-21 was cooled with a rate of 0.5 K s^{-1}; (c, d) DQ-145 and 146 were adopted with moderate cooling rates (2-3 K s^{-1}); (e, f) DQ-154 was quenched rapidly (25 K s^{-1}).

Figure 11 Spectra are shown to discuss possible hydrogen-deuterium isotope exchange between external fluid and inclusions. The Raman spectra (a) clearly show no contamination of the inclusion by D_2O. The FTIR spectra (b) in most cases show bands of H_2O as well as of D_2O due to possible incorporation of poor quality inclusions, e.g., necking-down inclusions (more details are given in text). Bands at 2800 - 3000 cm^{-1} are due to hydrocarbon species formed along sample preparation.

This is a preprint, the final version is subject to change, of the American Mineralogist (MSA)
Cite as Authors (Year) Title. American Mineralogist, in press.
DOI: https://doi.org/10.2138/am-2020-7114

Appendix

Table A1 Initial loading of all runs

Table A2 EMP analyses of SMIs in run DQ-21 (% *m/m*)

This is a preprint, the final version is subject to change, of the American Mineralogist (MSA)
Cite as Authors (Year) Title. American Mineralogist, in press.
DOI: https://doi.org/10.2138/am-2020-7114

899 **Tables**

900 Table 1 Experimental design of fluid inclusion synthesis

SNO	Capsule material	Initial loading (+ Qz cylinders)	$NaCl_{eq.}$ (wt%)	t_1 (d)	t_2 (d)	Quench Technique	Cooling rate (K/s)	Inclusion type; Daughter mineral	Precipitates in capsule
±Cu ± Cu_2O + NaCl (Set 1)									
DQ-22	Cu	1 wt% NaCl +$SiO_{2(gel)}$	1.1	2	3	SQ	0.5	FI+SMI; Cu_2O	-
DQ-36	Cu	8 wt% NaCl	8.9	3	2	SQ	0.5	FI+SMI; Cu_2O	-
DQ-21	Cu	8 wt% NaCl +$SiO_{2(gel)}$	8.7	2	3	SQ	0.5	FI+SMI; Cu_2O	-
DQ-145	Cu	8 wt% NaCl +$SiO_{2(gel)}$	8.5	3	3	SQ+RQ	0.5; 25	FI+SMI; Cu_2O	-
DQ-146	Cu	8 wt% NaCl +$SiO_{2(gel)}$	8.3	3	3	CAQ	3	FI+SMI; Cu_2O	-
DQ-154	Cu	8 wt% NaCl +$SiO_{2(gel)}$	8.7	4	4	RQ	25	FI+SMI; Cu_2O	-
DQ-183	Cu	8 wt% NaCl +$SiO_{2(gel)}$	8.5	-	2	RQ	25	FI+SMI; Cu_2O	-
DQ-165	Cu	8 wt% NaCl +$SiO_{2(gel)}$	8.5	2	10	RQ	25	FI+SMI; Cu_2O	-
DQ-23	Cu	20 wt% NaCl +$SiO_{2(gel)}$	20.2	2	3	SQ	0.5	FI+SMI; Cu_2O	-
DQ-121	Cu	8 wt% NaCl +$SiO_{2(gel)}$	n.m.	2	7	SQ	0.5	FI+SMI; Cu_2O	-
DQ-187	Au	8 wt% NaCl+ $Cu_2O_{(s)}$ + $SiO_{2(gel)}$	6.8	2	5	SQ	0.5	FI; CuCl	Little CuCl
DQ-188	Au	8 wt% NaCl+ $Cu_2O_{(s)}$ + $SiO_{2(gel)}$	6.8	-	10	SQ	0.5	FI; CuCl	Little CuCl
DQ-99	Au	8 wt% NaCl	8.0	3	3	SQ	0.5	FI	-
DQ-100	Au	8 wt% NaCl +$SiO_{2(gel)}$	8.1	3	3	SQ	0.5	FI	-
DQ-101	Au	8 wt% NaCl +Qz powder	8.0	2	4	SQ	0.5	FI	-
Cu ± CuCl± Cu_2O ± HCl (Set 2)									
DQ-123	Cu	0.5 m HCl +$SiO_{2(gel)}$	-	2	4	VSQ+RQ	0.07;25	FI; CuCl	Massive CuCl
DQ-42	Cu	1.5 m HCl	-	3	3	SQ	0.5	FI; CuCl	Massive CuCl
DQ-43	Cu	1.5 m HCl+$SiO_{2(gel)}$	-	3	3	SQ	0.5	FI; CuCl	Massive CuCl
DQ-169	Cu	1.5 m HCl + $Cu_2O_{(powder)}$+ $SiO_{2(gel)}$	-	3	3	RQ	25	FI; CuCl	Little CuCl
DQ-102	Cu	1.5 m HCl +H_2O+ $CuCl_{(s)}$ + $SiO_{2(gel)}$	-	3	3	RQ	25	FI; CuCl	Massive CuCl

DQ-47	Cu	H_2O+$CuCl_{(s)}$ + $SiO_{2(gel)}$	-	3	3	SQ	0.5	FI; CuCl	Little CuCl
Additional experiments (Set 3)									
DQ-37A	Cu	H_2O	-	3	2	SQ	0.5	FI	-
DQ-37B	Cu	H_2O (No Qz)	-	-	0.79	RQ	25	-	-
DQ-37C	Cu	H_2O (No Qz)	-	-	1.08	RQ	25	-	-
DQ-124	Au	D_2O (Qz from DQ121)	-	-	0.04	SQ	0.5	FI+SMI; Cu_2O	-

Notes:

All experiments were conducted at 800°C, 200 MPa. Two types of quartz cylinders were generally loaded unless otherwise mentioned (DQ-188 with only a pref. Qz, DQ-37B and 37C without Qz).

m denotes the molality of the solution, mol kg^{-1}.

$Cu_2O_{(powder)}$ and $Cu_2O_{(s)}$ refers to cuprite powder and sintered cuprite pellet, respectively.

In order to compare the bulk salinity from microthermometry measurements ($NaCl_{eq.}$) with the initial solution, we used wt% instead of molality of NaCl solutions. The conversion between wt% and molality is: 1wt% = 0.17 m $NaCl_{aq}$, 8 wt% = 1.49 m $NaCl_{aq}$, 20 wt% = 4.30 m $NaCl_{aq.}$

t_1 denotes experiment duration before intermediate quench, t_2 refers to the run duration after intermediate quench. The runs DQ-183 and DQ-188 were not conducted with intermediate quench.

Quench techniques: *CAQ* - compressed air quench; *RQ* - rapid quench; *SQ* - slow quench; *VSQ+RQ* - very slow quench and rapid quench (for more details see *Experimental and analytical procedure*).

FI represents fluid inclusion, *SMI* represents silicate melt inclusion.

This is a preprint, the final version is subject to change, of the American Mineralogist (MSA)
Cite as Authors (Year) Title. American Mineralogist, in press.
DOI: https://doi.org/10.2138/am-2020-7114

914 Table 2 The composition of the fluid phase in the conducted experiments

SNO	pH	$Cl_{tot.}$ m	Quench fluid m	Cu (pref. Qz) m	FIs	Cu (i.s. Qz) m	FIs	Note
± Cu ± Cu_2O + NaCl (Set 1)								
DQ-22	7	0.17	n.m.	0.03 ±0.01	16	0.04±0.02	14	Na std.
DQ-36	13	1.49	n.m.	0.16±0.12	12	0.11±0.11	3	Na std.
DQ-21	7	1.49	n.m.	0.16±0.07	15	0.17±0.10	16	Na std.
DQ-145	n.m.	1.49	n.m.	0.14±0.06	15	‡		Na std.
DQ-146	13	1.49	n.m.	0.14±0.05	15	‡		Na std.
DQ-154	n.m.	1.49	n.m.	0.16±0.07	16	0.17±0.03	15	Na std.
DQ-183	8	1.49	n.m.	0.15±0.12	15	‡		Na std.
DQ-165	5.61[b]	1.49	1.56(Na)/0.002(Cu)	0.20±0.04	9	0.20±0.04	12	Na std.
DQ-23	8	4.28	n.m.	0.46±0.20	16	0.42±0.18	15	Na std.
DQ-187	7	1.49	n.m.	0.54±0.14	15	0.53±0.12	14	Rb std.
DQ-188	7	1.49	n.m.	0.43±0.17	15	‡		Rb std.
Cu ± CuCl± Cu_2O ± HCl (Set 2)								
DQ-123	3	0.5	n.m.	0.44±0.21	15	0.62±0.21	9	Rb std.
DQ-42	1	1.5	n.m.	0.82±0.36	12	1.23±0.37	16	Rb std.
DQ-43	1	1.5	n.m.	1.28±0.56	16	1.29±0.58	13	Rb std.
DQ-169	4.06[b]	1.5	0.09(Cu)	1.01±0.38	12	‡		Rb std.
DQ-102	3	1.88	n.m.	1.63±0.30	11	‡		Rb std.
DQ-47	1	1.45	n.m.	0.54±0.19	13	0.57±0.21	15	Rb std.
Additional experiments (Set 3)								
DQ-37A	4	0	n.m.	0.004±0.003	15	0.003±0.002	10	Rb std.
DQ-37B*	4.01[b]	0	0.02 (Cu)					
DQ-37C*	4.26[b]	0	0.04(Cu)					

915 Notes:

916 [b] pH of quench fluids is measured by an Inlab microelectrode, data presented are corrected
917 based on their dilution factors; other data are based on pH papers; *n.m.* denotes pH of the
918 quench fluids was not measured.

919 $Cl_{tot.}$ represents the initial Cl content (mol kg^{-1}).

Na and Cu in brackets represent concentrations determined by ICP-OES which yields a precision less than 10% (2SD).

Cu content of FI is the mean value from *n* individual fluid inclusion measurements by LA-ICP-MS analyses. Uncertainties represent 95% confidence intervals.

Na std. is based on $NaCl_{eq.}$ of microthermometric data; *Rb std.* is calculated using the initial RbCl content in starting solution.

‡ Inclusions are too small to be analyzed or no i.s. Qz was loaded (DQ-188).

This is a preprint, the final version is subject to change, of the American Mineralogist (MSA)
Cite as Authors (Year) Title. American Mineralogist, in press.
DOI: https://doi.org/10.2138/am-2020-7114

927 Supplementary tables

928 Table A1 Initial loading of all runs

SNO	Qz	$SiO_{2\ (gel)}$	$Cu_2O_{(s)}$	$CuCl_{(s)}$	$NaCl_{(aq)}$	$HCl_{(l)}$	$H_2O_{(l)}$	Cu^+ / Cl^- Min initial ratio
	10^{-3} g	10^{-3} g	10^{-3} g	10^{-3} g	10^{-3} g	10^{-3} g	10^{-3} g	
±Cu ± Cu_2O + NaCl (Set 1)								
DQ-22	48.79	2.41			25.07			
DQ-36	46.17				26.52			
DQ-21	47.50	1.73			24.49			
DQ-145	46.42	3.70			30.72			
DQ-146	38.85	2.38			30.16			
DQ-154	37.08	1.63			29.96			
DQ-183	33.56	2.34			31.21			
DQ-165	39.53	2.05			30.96			
DQ-23	46.91	2.22			27.56			
DQ-187	54.59	2.13	22.89		22.89			10.2
DQ-188	28.55	2.36	22.29		35.18			6.5
Cu ± CuCl± Cu_2O ± HCl (Set 2)								
DQ-123	41.61	3.91				9.94	20.15	
DQ-42	58.93					24.10		
DQ-43	63.94	3.41				24.25		
DQ-169	62.50	3.25	3.67			28.51		1.2
DQ-102	34.82	2.20		3.13		15.50	14.59	0.6
DQ-47	52.44	2.58		4.37			30.43	1.0
Additional experiments (Set 3)								
DQ-37A	46.32						25.92	
DQ-37B							61.71	
DQ-37C							62.32	
DQ-99	16.07				30.69			
DQ-100	42.92	2.73			31.45			
DQ-101	41.87	2.44			26.24			

929 Note:

930 Stock solutions, such as $NaCl_{(aq)}$, $HCl_{(l)}$, are prepared prior to loading. Unless otherwise

931 mentioned, H_2O has not been added in each capsule.

932 The ratio of Cu^+/Cl^- denotes a minimum mole ratio between the initial Cu(I) minerals (CuCl,

933 Cu_2O) and chloride content.

934

This is a preprint, the final version is subject to change, of the American Mineralogist (MSA)
Cite as Authors (Year) Title. American Mineralogist, in press.
DOI: https://doi.org/10.2138/am-2020-7114

935 Table A2 EMP analyses of SMIs of DQ-21 (in wt%)

Sample	Na_2O	SiO_2	Cl	Cu_2O	Total
Cuprite	4.77	24.04	0.17	65.28	94.67
Cuprite	0.72	12.75	0.01	88.76	102.6
SMI-1	1.98	78.48	0.32	8.94	90.51
SMI-2	4.54	61.74	0.31	2.79	71.1
SMI-2*	1.95	68.86	0.32	0.06	74.04
SMI-2*	5.09	75.4	0.92	0.25	84.15
SMI-2*	2.04	70.59	0.23	0.95	76.67
SMI-3	3.9	81.11	0.04	-0.45	88.4
SMI-3*	-0.02	81.79	0.01	0.13	82.09
SMI-4	2.07	65.4	0.35	-0.16	71.47
SMI-5	4.12	63.95	0.05	-0.03	75.5
SMI-5*	1.88	60.35	0.04	0	71.81
SMI-5*	4.19	70.16	0.02	0.34	79.08

936 Notes: Cuprite refers to analyses on the small crystals, SMI refers to measurements on
937 glasses. A focused beam and a current of 15 nA were used for cuprite, a defocused bean
938 with a size of 2 μm and a current of 5 nA were used for glasses. * indicates analyses on the
939 same inclusion but at different locations.

940

This is a preprint, the final version is subject to change, of the American Mineralogist (MSA)
Cite as Authors (Year) Title. American Mineralogist, in press.
DOI: https://doi.org/10.2138/am-2020-7114

941 **Figures**

942

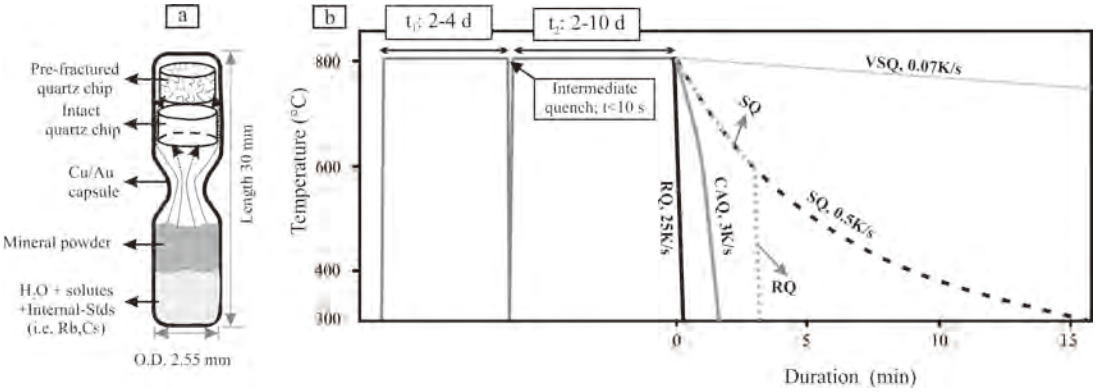

943

944 Figure 1 Schematic drawing of the experiment conducted in RH/RQ Ar-CSPV. (a) The
945 design of capsule, which is modified after Derrey et al. (2017); (b) Thermal history of the
946 experiment. The cooling rates were calculated based on the total time needed for the
947 temperature dropping from 800°C to 300°C at the external thermocouple.

948

949

This is a preprint, the final version is subject to change, of the American Mineralogist (MSA)
Cite as Authors (Year) Title. American Mineralogist, in press.
DOI: https://doi.org/10.2138/am-2020-7114

950

951

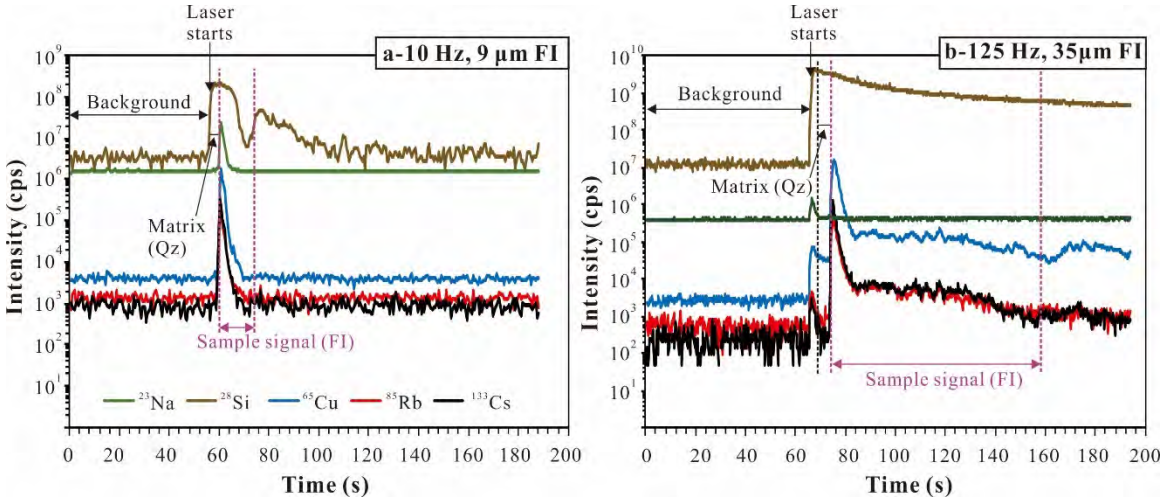

952

953 Fig.2 Typical LA-ICP-MS signals of small (a) and large (b) frozen FIs using a UV-fs-laser,
954 heating-freezing cell and *Element XR* ICP-MS. (a) Small FI has been ablated by spot
955 ablation pattern. DQ21: Cu+$SiO_{2(gel)}$+1.49 m $NaCl_{aq}$. (b) Large FI has been ablated by
956 spiral ablation pattern. DQ36: Cu+1.49 m $NaCl_{aq}$.

957

958

959

This is a preprint, the final version is subject to change, of the American Mineralogist (MSA)
Cite as Authors (Year) Title. American Mineralogist, in press.
DOI: https://doi.org/10.2138/am-2020-7114

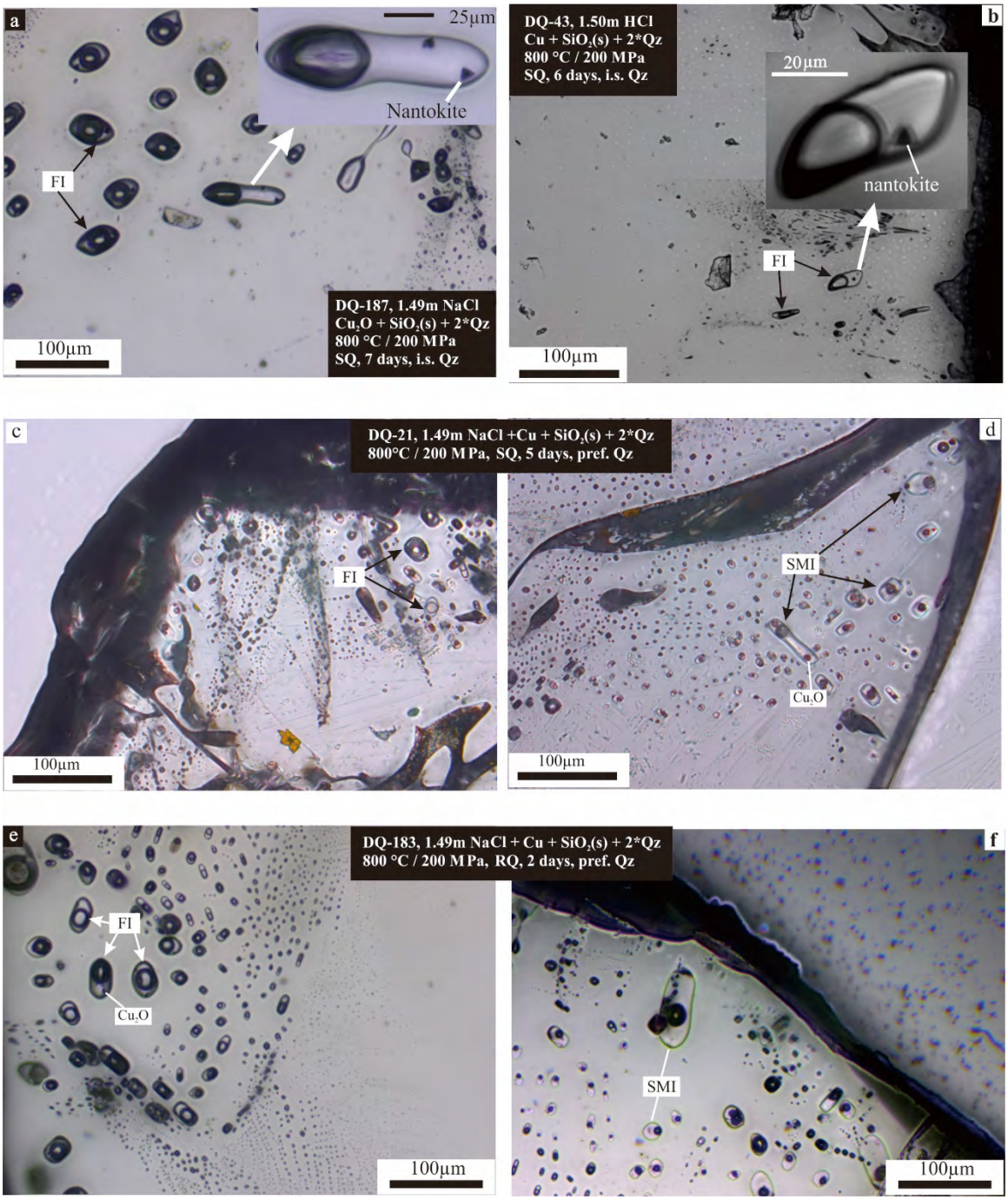

Figure 3 Photomicrographs of typical quartz-hosted inclusions at 25°C. (a) Nantokite was observed in FIs of the run with cuprite (Cu_2O) and NaCl solution (DQ-187); (b) Potential nantokite was precipitated in FIs of the run with native Cu and HCl solution (DQ-43). (c, d) Photos are taken from different area of the pref. Qz of DQ-21 in which FI (marked in (c)) coexists with SMI (marked in (d)). Discernible cuprite crystals are observed in SMI in

966 despite of FI. (e, f) Both FI and SMI occur in the pref. Qz of DQ-183, no intermediate
967 quench was adopted. FI often contains cuprite aggregates.
968

969

970

971

972

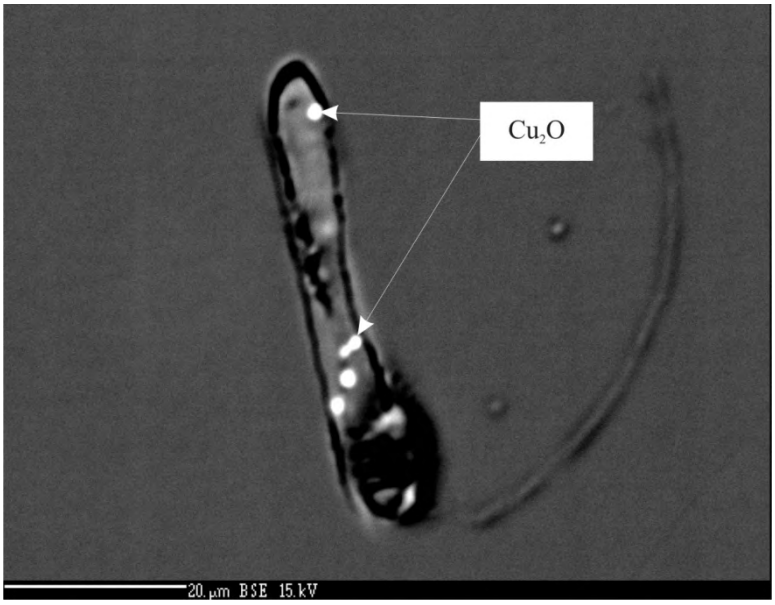

973

974 Figure 4 A BSE image of a SMI in pref. Qz of DQ-21. The rounded bright dots were

975 identified as cuprite using Raman spectroscopy (see Fig. 5a).

976

This is a preprint, the final version is subject to change, of the American Mineralogist (MSA)
Cite as Authors (Year) Title. American Mineralogist, in press.
DOI: https://doi.org/10.2138/am-2020-7114

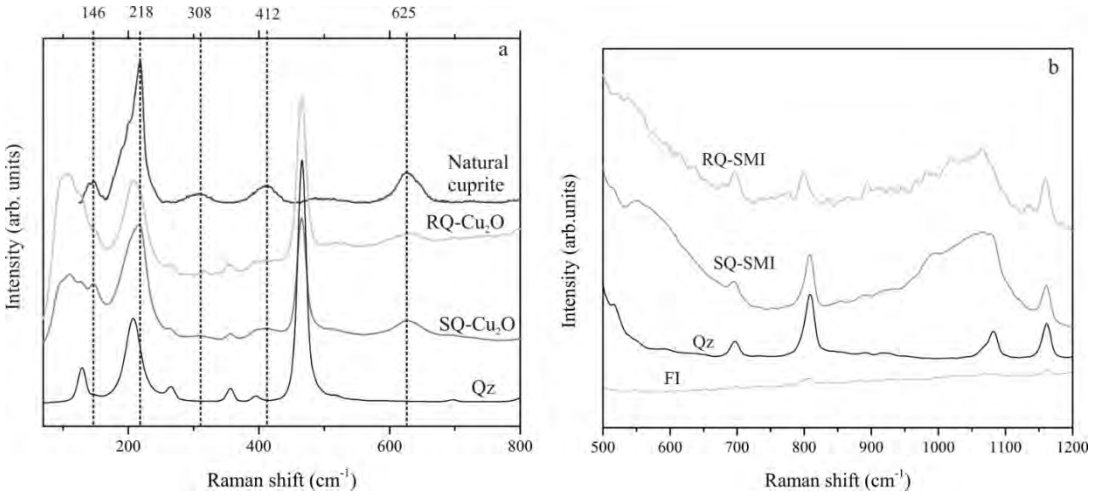

977

978 Figure 5 Raman spectra of different phases in inclusions after SQ (DQ-21) and RQ (DQ-
979 183) runs. (a) Raman analyses of crystals trapped in FIs (DQ-183) and SMIs (DQ-21) in
980 comparison with natural cuprite and quartz host. The vertical dashed lines are assigned to
981 typical cuprite Raman bands (for more details in text). (b) Raman analyses of silicate melt
982 phase in comparison to quartz and FI. Broad bands at 550-600 cm^{-1} and 1000-1100 cm^{-1}
983 may be assigned to amorphous silica (see text). *SQ* and *RQ* refer to runs and, respectively.

984

985

This is a preprint, the final version is subject to change, of the American Mineralogist (MSA)
Cite as Authors (Year) Title. American Mineralogist, in press.
DOI: https://doi.org/10.2138/am-2020-7114

986

987

988

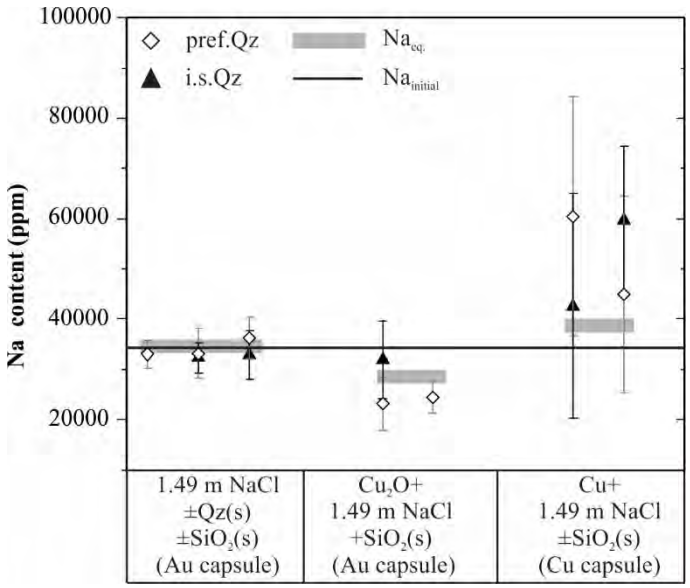

989

990 Figure 6 Examples of Na contents in FIs based on the internal standard Rb (400 μg g^{-1}).
991 The gray bar represents $Na_{eq.}$ which is evaluated Na content from microthermometry
992 measurement; $Na_{initial}$ denotes the initial Na content estimated from the starting solution.

993

994

This is a preprint, the final version is subject to change, of the American Mineralogist (MSA)
Cite as Authors (Year) Title. American Mineralogist, in press.
DOI: https://doi.org/10.2138/am-2020-7114

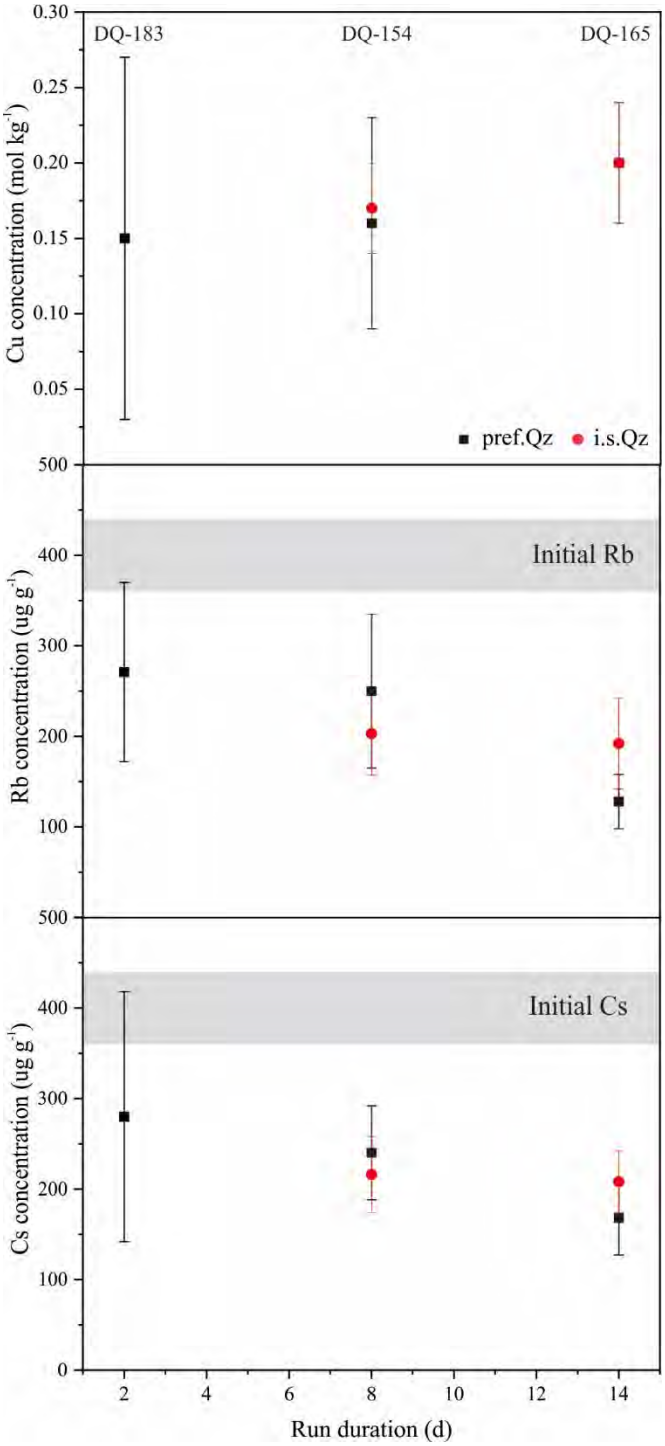

Figure 7 Average Cu, Rb and Cs concentrations of FIs (error bar is given by the standard deviation of the data). All runs were conducted with same material and same condition using rapid quench technique. Intermediate quench was performed after 0 (DQ-183), 2 (DQ-154) and 4 (DQ-165) d.

This is a preprint, the final version is subject to change, of the American Mineralogist (MSA)
Cite as Authors (Year) Title. American Mineralogist, in press.
DOI: https://doi.org/10.2138/am-2020-7114

1000

1001

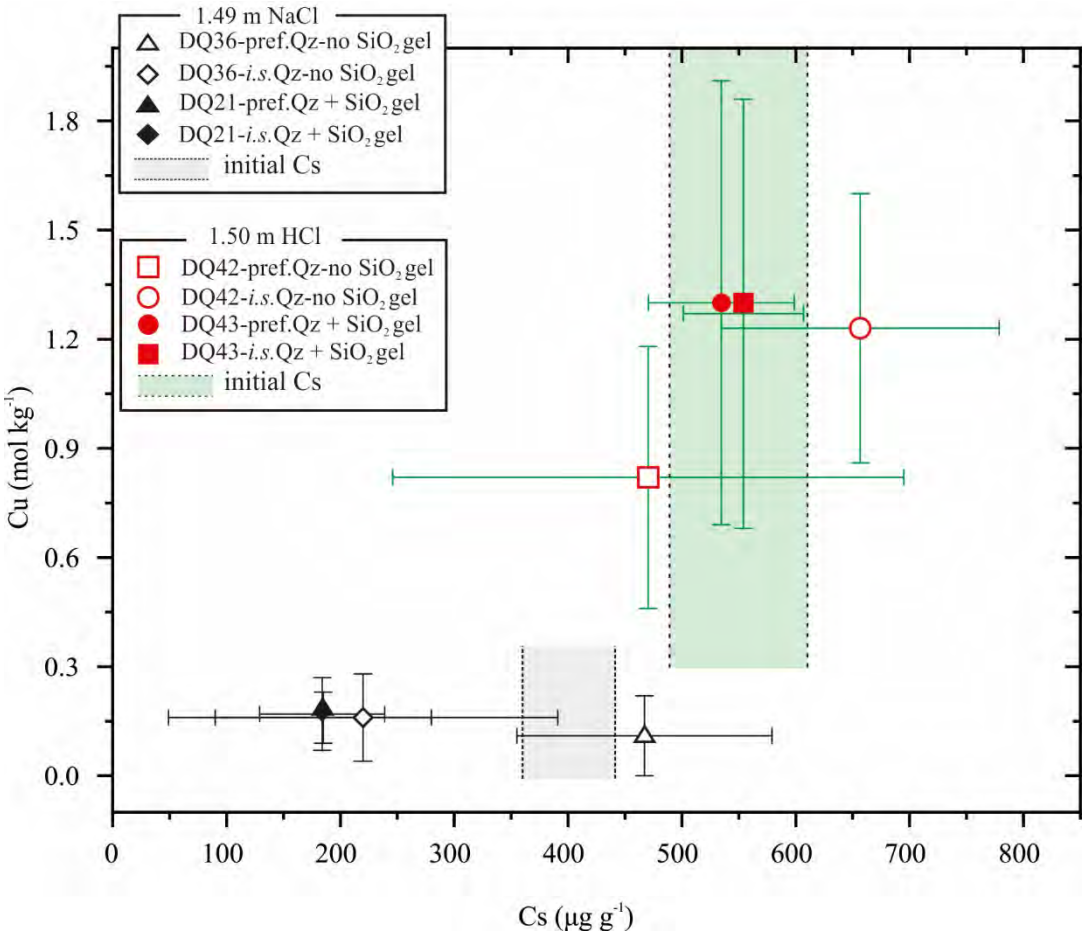

1002

1003 Figure 8 Cu content versus Cs content in Na^+ bearing and Na^+ free runs using SQ technique.

1004

This is a preprint, the final version is subject to change, of the American Mineralogist (MSA)
Cite as Authors (Year) Title. American Mineralogist, in press.
DOI: https://doi.org/10.2138/am-2020-7114

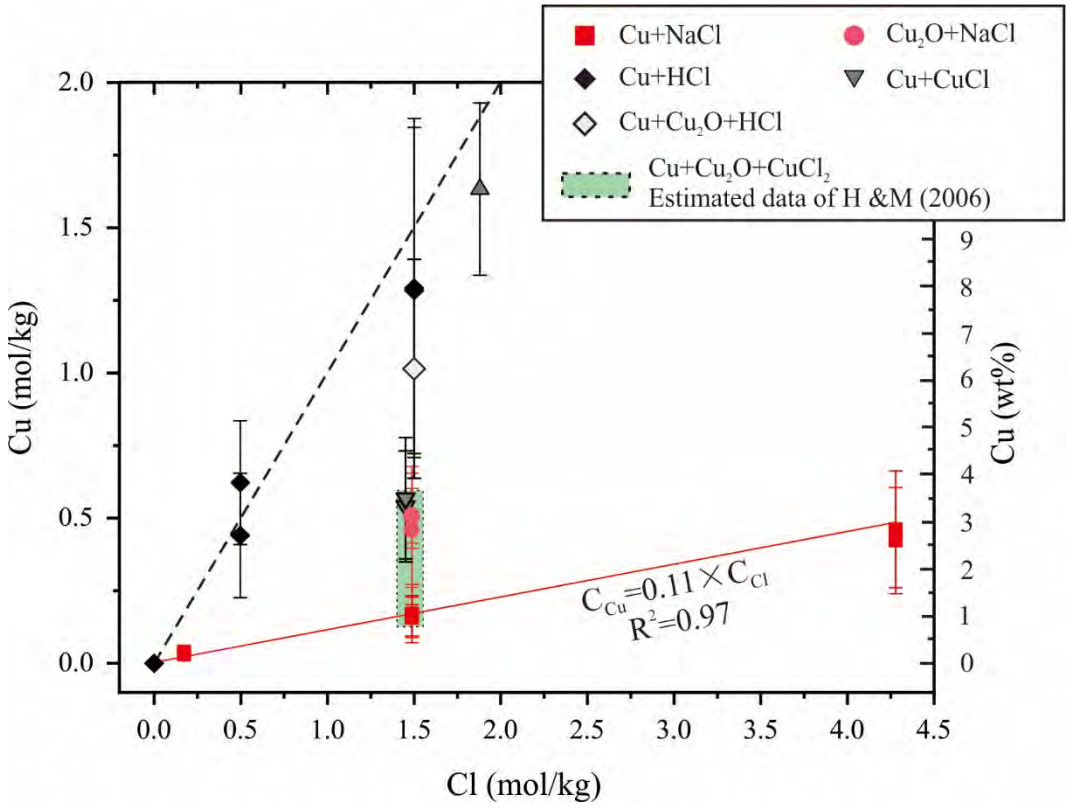

Figure 9 Cu concentrations as a function of initial chloride concentration in Cu±Cu_2O±CuCl±NaCl±HCl systems. All runs were performed in Cu capsules with cooling rate of 0.5 K s^{-1}, except for the run with Cu_2O+NaCl (Au capsule). Red symbols represent the runs with NaCl solution, whereas other symbols stand for the runs with Na-free solution. Solid line is a regression relation between the average Cu concentration derived from Cu+NaCl system and initial chloride concentration. Dashed line represents Cu/Cl ratio of 1:1.

This is a preprint, the final version is subject to change, of the American Mineralogist (MSA)
Cite as Authors (Year) Title. American Mineralogist, in press.
DOI: https://doi.org/10.2138/am-2020-7114

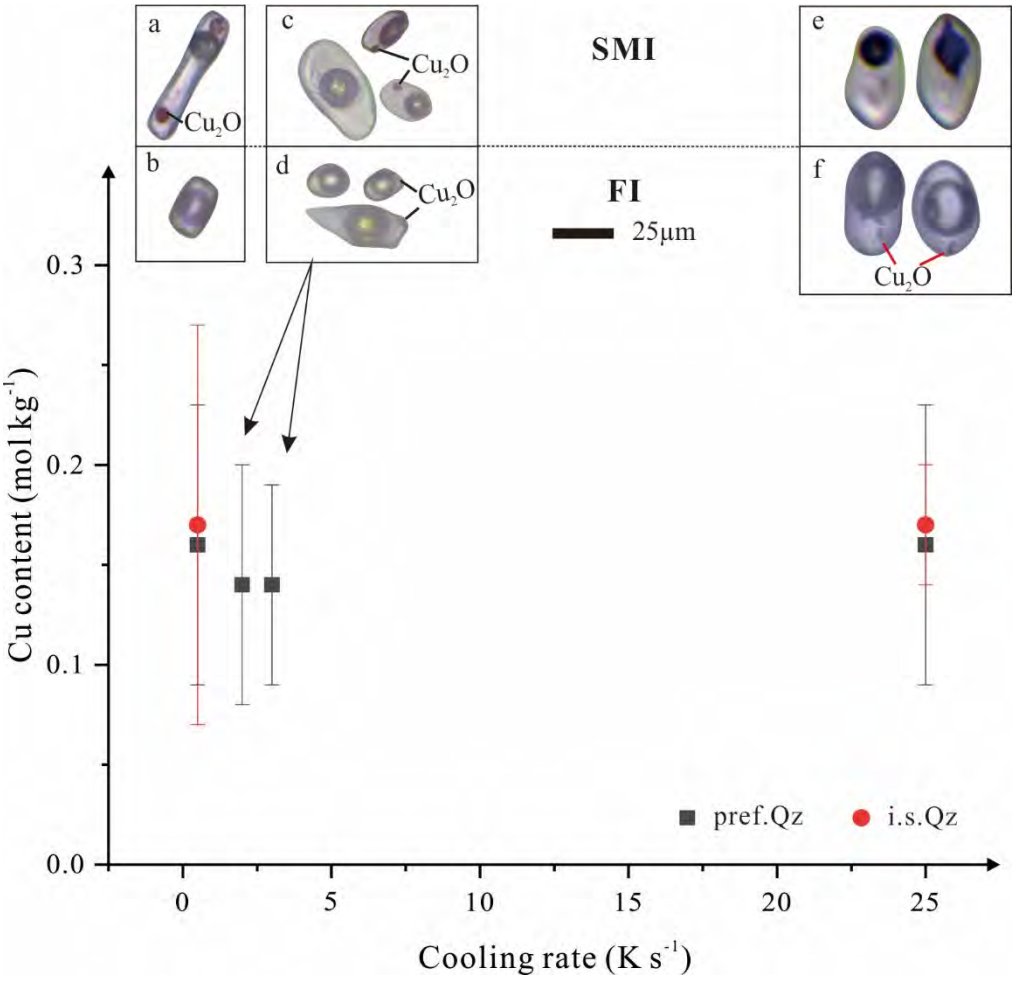

Figure 10 Cu content of FIs as a function of cooling rate, and the presence of cuprite in FIs and SMIs with respect to cooling rate. All runs were conducted in Cu+1.49 m NaCl system. (a, b) DQ-21 was cooled with a rate of 0.5 K s^{-1}; (c, d) DQ-145 and 146 were adopted with moderate cooling rates (2-3 K s^{-1}); (e, f) DQ-154 was quenched rapidly (25 K s^{-1}).

This is a preprint, the final version is subject to change, of the American Mineralogist (MSA)
Cite as Authors (Year) Title. American Mineralogist, in press.
DOI: https://doi.org/10.2138/am-2020-7114

1025

1026

1027

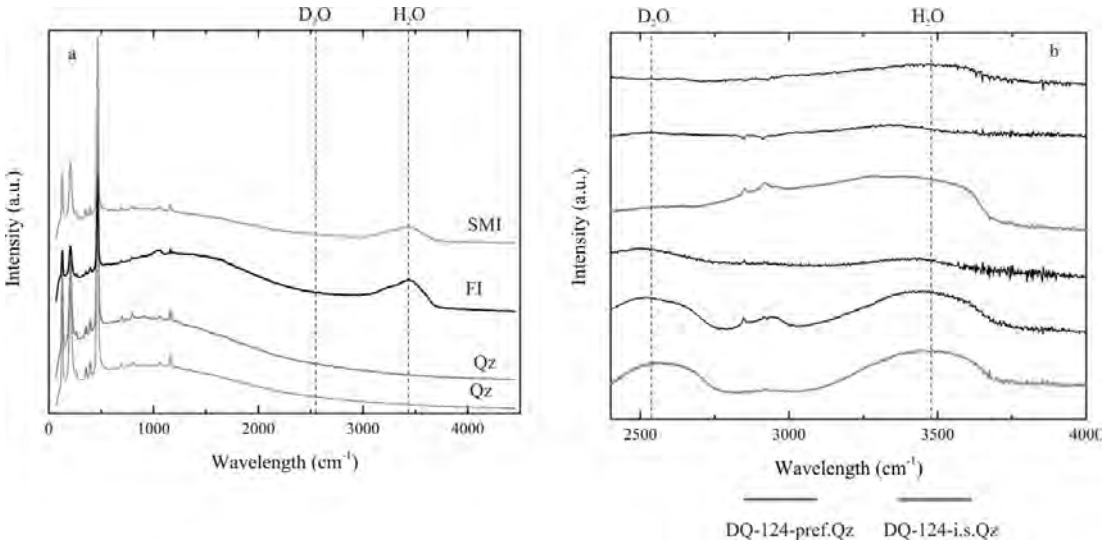

1028

1029 Figure 11 Spectra are shown to discuss possible hydrogen-deuterium isotope exchange
1030 between external fluid and inclusions. The Raman spectra (a) clearly show no
1031 contamination of the inclusion by D_2O. The FTIR spectra (b) in most cases show bands of
1032 H_2O as well as of D_2O due to possible incorporation of poor quality inclusions, e.g.,
1033 necking-down inclusions. Bands at 2800 - 3000 cm^{-1} are due to hydrocarbon species
1034 formed along sample preparation.

1035